Analysis of CF3I quasicontinuum states. III

C. Angelie

Citation: The Journal of Chemical Physics **98**, 9284 (1993); doi: 10.1063/1.464409
View online: http://dx.doi.org/10.1063/1.464409
View Table of Contents: http://scitation.aip.org/content/aip/journal/jcp/98/12?ver=pdfcov
Published by the AIP Publishing

Analysis of CF_3I quasicontinuum states. III

C. Angelie
Commissariat à l'Energie Atomique, Centre d'Etudes Nucleaires de Saclay, DSM/DRECAM/Service de Photophysique Atomes et Molecules, 91191 Gif sur Yvette Cedex, France

(Received 13 October 1992; accepted 1 March 1993)

CF_3I quasicontinuum (QC) states are analyzed in the framework used previously for SF_6 in papers I and II of this series. The existence of a hierarchy of intramolecular couplings V_k, decreasing vs the number k of vibrational quanta exchanged, with an effective density of coupled states ρ_k, is pointed out. The oscillator strength redistribution is described taking into account isolated resonances and perturbative redistribution associated to the lowest orders k, dissipative redistribution associated to higher orders, multiple transitions, and mode inhomogeneous spreading. Published homogeneous spectra of $^{12}CF_3I$ and $^{13}CF_3I$ at $E=19\,000$ cm^{-1}, near the dissociation threshold, are reinvestigated in this framework and a new assignment of the resonances is proposed. Using fluorescence data at $\langle E\rangle=3200$ cm^{-1}, an interpolation of the position and weight of the main resonances ν_1, ν_4, $\nu_2+\nu_3$, $2\nu_5$, in the frequency range 900–1200 cm^{-1}, becomes possible. This interpolation allows to extract from IR multiphoton absorption data, at the laser frequency $\nu_L=1072$ cm^{-1}, an average Lorentzian half-width $\bar{\gamma}$ ($\langle n\rangle$) vs the average number of photons absorbed $\langle n\rangle$. $\bar{\gamma}$ increases from 1 to 5 cm^{-1} for $\langle n\rangle$ varying from 5 to 10, and varies slowly around 4–5 cm^{-1} for $10\leqslant\langle n\rangle\leqslant 18$. Finally, the onset of the QC, near $E\sim 6000$ cm^{-1}, is explained using a modelization of the hierarchy V_k, ρ_k, without arbitrary parameters, and an intramolecular relaxation time $\sim$20 ps is predicted. This analysis leads to a very good agreement between the different sets of data concerning the CF_3I molecule.

I. INTRODUCTION

In the first paper of this series,[1] IR fluorescence data have been reported for SF_6, and to a less extent for CF_3I, excited at high vibrational energies. Owing to a high sensitive device, it was possible to observe the out of resonance redistributed fluorescence. This one could not be interpreted in the framework of a simple Bixon–Jortner[2] (BJ) model assuming constant couplings of density ρ, which leads to Lorentzian spectra with a half-width $\gamma=\pi\rho V^2$. The presence of a hierarchy of intramolecular couplings V_k, ordered by a rank k corresponding to the number k of vibrational quanta exchanged, was obvious. The most striking fact was that the strongest couplings, and lowest orders $k=3,4$, are only able to produce isolated perturbative resonances, or accidental strong resonances, owing to a too much small effective density of states ρ_k. More definitely, the condition $\pi\rho_k V_k<1$ is checked. Then, a description of the intramolecular vibrational redistribution (IVR), more suitable than the BJ model, was necessary, and explained in Ref. 3 (hereafter referred to as paper II of this series). The main results are recalled in Sec. II. Lorentzian expressions of the resonances remain formally valid with a parameter γ having fluctuations. We have called this description a "quasi-Lorentzian" formalism.

Using this description of the IVR, the various data available about SF_6, the most studied molecule in the field of IR multiphoton absorption (IRMPA), have been reinvestigated in paper II. An impressive agreement has been obtained between the different informations: fluorescence data,[1] IRMPA data at the laser frequency $\nu_L=944$ cm^{-1}, in the nanosecond regime,[4] or in the picosecond regime,[4–5] Raman monitoring of the QC threshold[6–8] ($E_{QC}\sim 4000$ cm^{-1}), IRMPA data with a high pressure CO_2 laser, and a varying laser linewidth.[9] For example, a modelization of the couplings hierarchy V_k, ρ_k, with parameters fixed by fluorescence data, explains the value $E_{QC}=4000$ cm^{-1} ± 500 cm^{-1}; fluorescence and IRMPA data give the same average value of the parameter $\gamma=\pi\rho V^2\sim 4$–5 cm^{-1} at $E=11\,000$–$18\,000$ cm^{-1}; the modelization of the hierarchy predicts a relaxation time $T_1\sim 13$ ps near the QC onset, while picosecond experiments provide $T_1\sim 11$ ps.[4]

CF_3I is the second most studied molecule in the IRMPA field, and we try, in this paper, to obtain a general description of its known properties, in the same framework as for SF_6. The success of this framework, for the two benchmark molecules of the IRMPA process will be the clue that the essential features of QC states are understood. The experimental data are nevertheless a little less numerous for CF_3I. No picosecond data are available. Fluorescence data have been obtained only at $\langle E\rangle=3200$ cm^{-1} in Ref. 1, either for $^{12}CF_3I$ or $^{13}CF_3I$, but they provide useful constants about the anharmonic shifts and couplings for the main resonances ν_1, ν_4, $\nu_2+\nu_3$, and $2\nu_5$. In any case, there exist numerous data about IRMPA or IRMPD (dissociation) properties. IRMPA data and simultaneous Raman monitoring of the QC threshold ($E_{QC}\sim 6000$ cm^{-1}), or of the fraction q of molecules excited above E_{QC}, can be found in Refs. 6–8. IRMPA data with a high pressure CO_2 laser of varying laser linewidth are also available, either for the ^{12}C or for the ^{13}C species.[9] Last but not least, unique spectra have been obtained for the CF_3I molecule at $E=19\,000$ cm^{-1}, near the dissociation threshold, using a two laser frequency photodissociation method, either for $^{12}CF_3I$ (Refs. 10 and 11) or $^{13}CF_3I$ (Ref. 12). This method allows to reduce the inhomogeneous contribution of the linewidth, due to the spreading of the monitored distribu-

 0021-9606/93/129284-19$06.00

tion vs the initial energy, to less than 3 cm^{-1}. A few resonances are clearly visible with half-linewidths γ varying from 2 to 19 cm^{-1}, according to the resonance. Owing to the remarkably narrow inhomogeneous contribution, these half-linewidths are clearly homogeneous and related to the intramolecular redistribution process.

An assignment of the resonances of the homogeneous spectra at $E=19\,000$ cm^{-1} was proposed in Refs. 10–12. We show in Sec. III that this assignment raises several difficulties. Particularly, an isotopic selectivity observed in SF_6/CF_3I photosensitized dissociation experiments[13–15] are not explained within this assignment. We propose in Sec. III a new assignment which solves practically all difficulties. From this description at $E=19\,000$ cm^{-1}, and the fluorescence data at $\langle E\rangle=3200$ cm^{-1}, it becomes possible to interpolate with good confidence the position and weight of the different main resonances, in the frequency range 900–1200 cm^{-1}.

In Sec. IV we use this prediction of the oscillator strength distribution to extract an average parameter $\bar{\gamma}(E)$ from CF_3I IRMPA data. Such an extraction had been attempted in Ref. 16, from CF_3I IRMPD data, using a Lorentzian description of the ν_1 oscillator strength redistribution. A value $\gamma=116$ cm^{-1} was obtained at $E=19\,000$ cm^{-1}. This value has been clearly ruled out by the subsequent direct observation of homogeneous photodissociation spectra reported in Refs. 10–12, which give values more than 1 order of magnitude smaller. This raises the question if the IRMPA (or IRMPD) process in the QC is correctly understood. The failure of the extraction performed in Ref. 16 is analyzed and it is shown that the new description of the resonances leads to a complete agreement with photodissociation data. Finally, a modelization of the hierarchy V_k, ρ_k, analogous to that used for SF_6 in Ref. 3, is explored in Sec. V. The sharing of the parameter γ between a perturbative and a dissipative part is analyzed, and the QC onset derived as well as the IVR time.

II. DESCRIPTION OF QC STATES

We summarize briefly the description of QC states used in Ref. 3, generalizing the BJ model, when a hierarchy of couplings V_k, with an effective density of coupled states ρ_k, is present. In the BJ model, for a doorway state $|s\rangle$ of average energy E_s formed from an initial state of energy E, for constant couplings V, and constant spacings $\epsilon=1/\rho$ of bath states, the redistributed oscillator strength is the Lorentzian function

$$L(E')=\rho\frac{1}{\pi}\frac{\gamma}{(E'-E_s)^2+\gamma^2+V^2} \tag{1a}$$

with

$$\gamma=\pi\rho V^2, \tag{1b}$$

where V, ρ, and γ can depend on the energy E_s but not on the final energy E'.

For a half-width γ of the Lorentzian function, the weight of the doorway state $|s\rangle$ relaxes exponentially with a time constant τ_{intra} given by

$$\tau_{\text{intra}}\times 2\gamma=5.3 \text{ ps } cm^{-1}. \tag{1c}$$

The term V^2 in the denominator of Eq. (1a) is often neglected but it determines the extension of the redistribution of $|s\rangle$. The number N of states involved in the redistribution can be obtained writing $L(E_s)=(1+N)^{-1}$. Then

$$N=(\pi\rho V)^2, \tag{2}$$

where $\pi\rho V<1$ corresponds to a perturbative redistribution. Then, V^2 is dominant in the denominator of Eq. (1a) and γ cannot be interpreted as a Lorentzian half-linewidth. $\pi\rho V>1$ corresponds to a dissipative redistribution. In this case, γ^2 is dominant in the denominator of Eq. 1(a) and it is really the half-linewidth of the function, implying an exponential relaxation vs time, according to Eq. (1c). The doorway state $|s\rangle$ is formed from an eigenstate $|E\rangle$ by a transition operator d (usually the dipole moment): $|s\rangle\propto d|E\rangle$.

The exact Hamiltonian H admits a zero order separable approximation H_0, with separable eigenstates $|\ldots v_i, l_i,\ldots,R\rangle$. v_i is the number of vibrational quanta in the mode i; l_i is an additional quantum number for a mode with degeneracy $g_i>1$ (for example, the internal angular momentum); R groups rotational quantum numbers. In this separable description, the initial state $|E_0\rangle$ provides a spectrum of *multiple transition* $(\Delta l_i,\Delta R)$, represented in Fig. 1(a) for the absorption component $\Delta v_i=+1$. They are spread over a width $2\Delta_{mp}\sim 10$–20 cm^{-1} as justified in Appendix A.

We consider now the coupling operator V neglected so far: $H=H_0+V$. It is always possible to express H_0 so that terms quadratic vs the coordinates are diagonalized. Then, V introduces only couplings of ranks $k\geqslant 3$. As it was shown for SF_6, and will be checked for CF_3I in Sec. V, the lowest orders $k=3,4$ give the strongest couplings, but with a density ρ_k such that the perturbative criterion $\pi\rho_k V_k\leqslant 1$ is checked. Then, these orders produce only a perturbative redistribution of isolated clusters of multiple transitions, as represented in Fig. 1(b). The weight of these clusters declines as $|V_k|^2/\Delta\nu^2$ in agreement with the BJ model used separately for each order. However, and this will be the case for CF_3I, some resonances b can check accidentally $|V_b|\geqslant|\Delta\nu_b|$, so that they are strongly coupled to $|s\rangle$: The redistribution is now strong but limited to a small number of lines. Then the lowest orders $k=3,4$ produce a perturbative or limited redistribution which we label P-L.

The second class of couplings, smaller, but with a high effective density of coupled states, checks the criterion of dissipative redistribution and is responsible for the statistical IVR on the energy shell. It corresponds to higher orders $k\geqslant k_d$ and we label it D. It produces in fact two distinct spreadings of the oscillator strength. Each component of the doorway state is redistributed according to a Lorentzian function having a dissipative half-width γ_{diss}:

$$\gamma_{\text{diss}}=\sum_{k\geqslant k_d}\gamma_k \tag{3a}$$

with

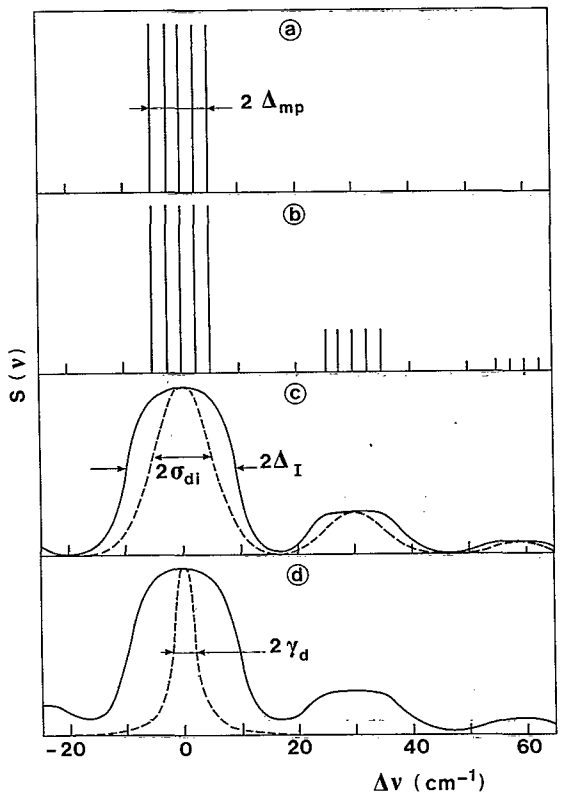

FIG. 1. Spectral redistribution of the oscillator strength in molecular QC states: (a) Splitting of the main line by multiple transitions; (b) perturbative or limited redistribution; (c) mode inhomogeneous spreading (the Gaussian dispersion is represented for one line by the dashed curve); (d) dissipative redistribution (the Lorentzian spreading for a given central frequency is represented by a dashed curve).

$$\gamma_k=\pi\rho_k V_k^2, \tag{3b}$$

i.e., γ_{diss} incorporates only the terms checking the dissipative condition. For SF_6, γ_{diss} was estimated to be around 1 cm^{-1}. However, the Lorentzian function describing the redistribution is centered on a frequency fluctuating vs the quantum numbers v_i for a total initial energy E. The resulting redistribution of the oscillator strength, for a resonance i, is therefore a convolution

$$S_i(\nu_L)=\bar{S}_i\int du\, I(u)\,\frac{1}{\pi}\,\frac{\gamma_{\text{diss}}}{[\nu_L-\nu_i(E)-u]^2+\gamma_{\text{diss}}^2}. \tag{4}$$

$I(u)$ represents the distribution of fluctuations and can be approximated by a Gaussian function with a half-width σ_{di} proportional to the energy. For CF_3I, σ_{di} is estimated to be ~ 5 cm^{-1} near the dissociation energy $E_d\sim 19\,000$ cm^{-1} (Appendix A). This spreading σ_{di} can be understood as a *mode inhomogeneity*[17–19] and it is represented in Fig. 1(c). The Lorentzian spreading related to γ_{diss} is represented in Fig. 1(d) and is mainly visible in the wings of the redistribution.

From the previous picture, it appears that the oscillator strength redistribution has not in general a Lorentzian shape. However, the Lorentzian expression remains useful provided some adaptation and reinterpretation are made and we call it the quasi-Lorentzian formalism. First, strong but limited redistribution must be treated by a set of separate resonances. But each one of these resonances can be treated formally by a Lorentzian function as in Eq. (1a) with a parameter γ depending smoothly on the final energy E':

$$\gamma(E\to E')=\pi\rho(E')\,|V(E\to E')|^2. \tag{5}$$

What makes this formal expression useful is that γ fluctuates practically within moderate limits vs E', as shown for SF_6 in papers I and II. This can be seen in the following way. Around resonance, $\gamma(E\to E')$ has the meaning of a half-width and is practically dominated by multiple transitions and mode inhomogeneous spreading, with a total width $\Delta_I\sim 10$ cm^{-1}, while γ_{diss} has a magnitude ~ 1 cm^{-1} [see Figs. 1(c) and 1(d)]. Then

$$\gamma\sim\Delta_I. \tag{6a}$$

Out of resonance, the maxima of $\gamma(E\to E')$ correspond to the perturbative resonances coupled by the matrix element V_{si} spread by multiple transitions and mode inhomogeneity [Fig. (1a)]. Then

$$\gamma\sim\pi\frac{|V_{si}|^2}{2\Delta_I}. \tag{6b}$$

For $V_{si}\sim 10$ cm^{-1} and $\Delta_I\sim 10$ cm^{-1}, we get $\gamma\sim 15$ cm^{-1}. Out of resonance, the minima depend on the overlap between the different perturbative resonances, but we have a minimum bound:

$$\gamma>\gamma_{\text{diss}}, \tag{6c}$$

i.e., $\gamma\gtrsim 1$ cm^{-1}. Equations (6) indicate the fluctuation bounds of $\gamma(E')$, over frequency scales $\sim 2\Delta_I$.

To use the quasi-Lorentzian formalism, it is necessary to have more definite expressions of the parameters. We indicate here the useful results of Ref. 3. The main aspects can be understood using a separable approximation H_0 quadratic in the vibrational quantum numbers, and with a rigid symmetric top rotational part.[20] Details are given in Appendix A.

The central transition frequency $\nu_i(E)$ of an absorption band $v_i\to v_i+1$, i.e., the part depending only on the total energy, can be expressed by[3,20]

$$\nu_i(E)=\nu_i(0)-a_iE+b_iE^2 \tag{7}$$

$\nu_i(0)$ and a_i are derived from the low levels spectroscopy. The last term gives a quadratic anharmonic shift.

The coefficient b_i is negative, $\sim 10\%$ of the linear part near the dissociation threshold, in the hypothesis of a quadratic Hamiltonian. However, the CF_3I spectroscopy at $E=19\,000$ cm^{-1} obtained in Refs. 6–8 shows that the term b_iE^2 is, in fact, positive and $\sim 30\%$ of the linear part, so that in the following b_i will be considered as an adjustable parameter. The contribution b_iE^2 remains small up to the half dissociation but is not negligible above.

With the previous expressions, informations can be obtained, from a local or averaged parameter γ, on the magnitude of the couplings V_k. It is useful to modelize the V_k hierarchy, in the spirit of the restricted quantum exchange

TABLE I. Spectroscopic coefficients of the low energy levels, extracted from Refs. 1 and 26–29.

Res	$\nu_i(0)$ (cm^{-1}) 12	13	a_i (10^{-3})	V_{1i} (cm^{-1}) E (cm^{-1})= 0	3200	K_i 10^{-20} cm^2
ν_1	1075.2	1047.6	5.2			
$\nu_2+\nu_3$	1029.7	1022.8	3.8	8.2	16.5	8.855
$2\nu_5$	1079.7	1076.8	8.0	2.6	12.5	
ν_4	1187.5	1154.3	6.5			6.224
Min	ν_m=1113 (E=3200 cm^{-1})				~10	

theory (RQET) of Stone *et al.*,[21–25] in which an exponential decrease is assumed: $V_k=V_0/a^k$. The knowledge of V_3 and V_4 fixes the two parameters V_0 and a (which can be dependent on the energy E).

III. ANALYSIS OF THE CF_3I SPECTRUM AT E=19 000 cm^{-1}: POSITION AND WEIGHT OF THE RESONANCES VERSUS ENERGY

A. Fluorescence data at $\langle E\rangle$=3200 cm^{-1}

We summarize in Table I the parameters obtained in Ref. 1 from the CF_3I fluorescence spectrum at $\langle E\rangle$=3200 cm^{-1}, which are useful for the discussion of the photodissociation spectrum at E=19 000 cm^{-1}. The ground level data (E=0) are also indicated and extracted from Refs. 26–29. $\nu_i(0)$ (Ref. 28) is indicated, either for the ^{12}C or for the ^{13}C isotope. It has been checked in Ref. 1, that the anharmonic shifts tally very well with the linear part computed with the coefficients X_{ij} of Ref. 26. Two Fermi resonances are clearly visible in the fluorescence spectra either for $^{12}CF_3I$ or $^{13}CF_3I$: $\nu_2+\nu_3$ and $2\nu_5$. The effective coupling V_{1i} with the ν_1 mode is indicated at E=0 (Ref. 28) or $\langle E\rangle$=3200 cm^{-1} (Ref. 1). The analysis of the two isotopic species ^{12}C and ^{13}C makes much easier the extraction of these couplings. The integrated cross section of the $\nu_1/\nu_2+\nu_3/2\nu_5$ and of the ν_4 resonances are indicated.[27,29] The values of Ref. 29 are chosen, which agree with those of Ref. 27 within a few percents. Finally several other parameters are useful. The CF_3I rotational coefficients[28] are A=0.1921 cm^{-1}, B=0.0508 cm^{-1}. The spherical splitting of the ν_4 mode[26] is given by G_{44}=4.35 cm^{-1}. It is worthwhile to mention that the $^{12}CF_3I$ fluorescence spectrum has been recorded continuously from 950 to 1200 cm^{-1} and is never zero. Particularly, the frequency ν_m~1113 cm^{-1} corresponds to a minimum equidistant from the ν_1 and ν_4 resonances and cannot be accounted for by an inhomogeneous thermal spreading, which has too fast a decrease. However, it can be interpreted as a secondary resonance b (likely the $\nu_5+2\nu_3$) coupled to the ν_1 and ν_4 modes by an effective coupling V_{eb}, and spread by the thermal distribution over a width $2\Delta_I$~25 cm^{-1}. Using Eq. (6b) we get V_{eb}~10 cm^{-1}.

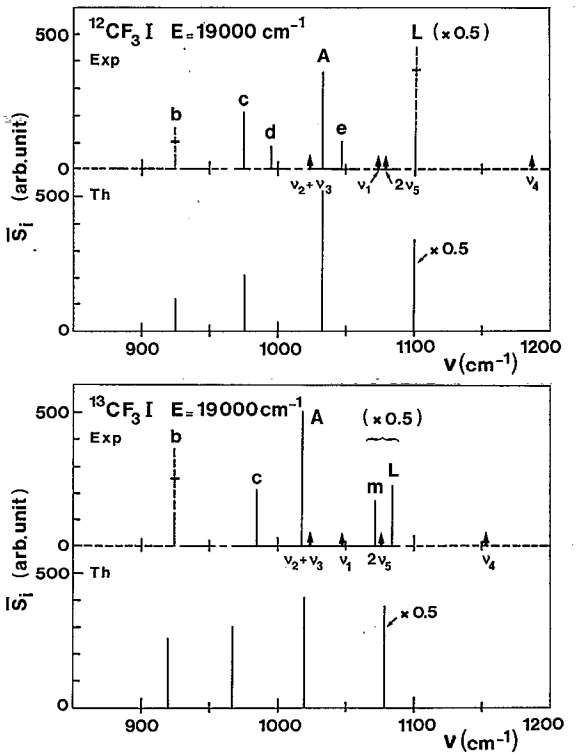

FIG. 2. Scheme of the photodissociation spectra of $^{12}CF_3I$ and $^{13}CF_3I$ near the dissociation threshold E=19 000 cm^{-1}. The positions ν of the resonances are indicated with their integrated cross section $\bar{S}_i$ (arbitrary unit). The arrows are the ground level frequencies. The upper parts (Exp) are the experimental data; the dashed parts in the abscissa axis indicate the unexplored ranges; the dashed parts on the resonances indicate interpolated oscillator strength. The lower parts (Th) represent the couplings model for the $\nu_1/\nu_2+\nu_3/2\nu_5$ multiplet.

B. Photodissociation spectrum at E=19 000 cm^{-1}

The photodissociation spectra reported in Refs. 10–12 for $^{12}CF_3I$ and $^{13}CF_3I$ at E=19 000 cm^{-1} are obtained in a molecular beam, at a rotational temperature T_{rot}~20 K, so that the rotational width does not exceed 2 cm^{-1}, which reduces strongly the multiple transitions spreading. The vibrational molecular inhomogeneity is reduced to ~2 cm^{-1}, owing to a two frequency differential dissociation method. Then all structures with widths greater than 3 cm^{-1} can be assigned to vibrational multiple transitions, vibrational mode inhomogeneity, and dissipative linewidth. Particularly, the mode inhomogeneous half-width σ_{di} has been estimated to be ~5 cm^{-1} at E=19 000 cm^{-1} for the ν_1 or ν_4 modes. It can be proved that these photodissociation spectra are proportional to absorption cross sections.

The diagrams of the $^{12}CF_3I$ and $^{13}CF_3I$ spectra obtained are represented in Fig. 2. The upper parts correspond to the experimental result. The position ν_i (cm^{-1}) and integrated intensity $\bar{S}_i$ (arbitrary unit) of each resonance are indicated. Unfortunately, due to the limited frequency range of $^{12}CO_2$ and $^{13}CO_2$ lasers, some interesting parts are missing. This is particularly true between 890 and 930 cm^{-1}, and for ν>1090 cm^{-1}, good interpolations being possible in the other ranges. Then some locations and weights of resonances can only be roughly estimated. The

TABLE II. Characteristics of $^{12}CF_3I$ and $^{13}CF_3I$ resonances at $E=19\,000$ cm^{-1}, labeled according to Fig. 1: central frequency ν_i, half-width γ_i, integrated absorption cross section $\bar{s}_i$, estimated effective coupling V_{ei} with the main resonance indicated in parentheses. The values of γ and V_e are also indicated for the frequency corresponding to the minimum between the peaks A and L/m.

	$^{12}CF_3I$					$^{13}CF_3I$			
Res	ν_i (cm^{-1})	γ_i (cm^{-1})	$\bar{S}_i$ (arb.)	V_{ei} (cm^{-1})	Res	ν_i (cm^{-1})	γ_i (cm^{-1})	$\bar{S}_i$ (arb.)	V_{ei} (cm^{-1})
A	1033	6	360		A	1018	19	505	
b	~925	<18	100 ±50	28±8 ($A+c$)	b	~920	>10	250 ±125	36±10 ($A+c$)
c	975	7	210	28 (A)	c	985	7.5	210	15 (A)
d	~995	5.5	85	9 (c)					
e	1047	2 (1.3)	105	6 (A)					
L	~1100	>15	>360		L	1082	6	450	
					m	1070	8.5	330	6 (L)
Min	1065	~10		~7	Min	1040	~10		~7

unexplored ranges are therefore represented by dashed lines in the upper abscissa axis. The positions of the main resonances ν_1, $\nu_2+\nu_3$, $2\nu_5$, and ν_4 in the ground level $E=0$ are indicated by arrows. In the $^{12}CF_3I$ spectrum, a great peak, noted A, is clearly visible as well as three secondary peaks, noted c, d, and e. The edges of a redistributed oscillator strength are visible near 890 and 930 cm^{-1}, so that a peak, noted b, can be assumed around 920–925 cm^{-1}. The minimum of the integrated cross section of this peak is indicated by the solid bar, and the dashed bar represents the probable uncertainty on the interpolation, with a hyphen indicating the most probable value. The beginning of another strong peak, noted as L, is visible around 1075–1090 cm^{-1}, but an important part is unexplored above 1090 cm^{-1}. The uncertainty is represented as for the peak b. The most probable value is computed assuming that this peak L is the anharmonically shifted ν_4 peak, in agreement with the interpretation of Refs. 10–12, and using the ratio of integrated cross-sections of Ref. 29: $\bar{S}_4/\bar{S}_1=0.78$. For the convenience of Fig. 2, the value $\bar{S}_L$ (~750) is multiplied by 0.5.

In the $^{13}CF_3I$ spectrum a broad peak is also visible, as well as a narrow peak, respectively comparable to A and c. The width of the peak A is too great to identify possible secondary peaks d or e. The edge of a peak, partly unexplored is clearly visible near 940 cm^{-1} and corresponds to the peak b also guessed on $^{12}CF_3I$. In the higher frequency part, two close peaks L and m are completely explored. An isotopic shift ~ -30 cm^{-1} allows now the complete exploration of the ν_4 peak, with a substructure m, what was not possible for $^{12}CF_3I$. This shows the great interest of an isotopic comparison to obtain a good assignment of the resonances. The main characteristics of the different peaks are gathered in Table II.

These characteristics deserve several remarks. The number of resonances in the range 900–1100 cm^{-1} is small, and can be assumed in strict correspondence with the lines known in the low levels, i.e., mainly the ν_1, ν_4, $\nu_2+\nu_3$, and $2\nu_5$ lines. The details of the assignment will be discussed in Sec. III C, but the basic interpretation developed in Refs. 10–12 will not be questioned. It rests on the identification of the resonance A with the ν_1 mode and the resonance L with the ν_4 mode. It is supported by several facts: They are the two strongest peaks, they exhibit an isotopic shift comparable to that of the ground level frequencies, and the ratio between the oscillator strengths $\bar{S}'_L$ of the peak L and its satellite m, and the oscillator strength $\bar{S}'_A$ of the peak A and its satellites b and c is $\bar{S}'_L/\bar{S}'_A \simeq 0.81$ for $^{13}CF_3I$, in close agreement with the ground level ratio:[29] $\bar{S}_4/\bar{S}_1 \simeq 0.78$. This ratio cannot be obtained for $^{12}CF_3I$ since the peak L is partially explored.

The peaks b, c, d, and e correspond to a redistribution of the ν_1 peak through intramolecular couplings, and the peak m to a redistribution of the ν_4 peak. Then, in spite of the high energy content, resonances keep their meaning, and some zero order separable Hamiltonian H_0 remains a good approximation up to the dissociation threshold. This was also checked for SF_6 in Ref. 1 up to the half-dissociation energy ($E=17\,000$ cm^{-1}).

The position of the resonance ν_4 shows, however, that the linear expression of the anharmonic shift, the term $-a_iE$ in Eq. (7), is not sufficient for CF_3I at $E=19\,000$ cm^{-1}: the value $a_i=6.5\ 10^{-3}$ (Table I) predicts a position of the $^{13}CF_3I$ ν_4 mode at $\nu=1031$ cm^{-1}, while it is observed at ~1076 cm^{-1} (middle frequency between L and m). Then, we must accept the presence of a nonlinear part $b_iE^2 \sim +45$ cm^{-1}, i.e., about one-third of the linear part. This fact fixes the value of b_i for the $^{13}CF_3I$ ν_4 mode ($b_4 = +12.5\times10^{-8}$ cm, for E in cm^{-1}). The coefficients b_i of the other resonances ν_1, $\nu_2+\nu_3$, $2\nu_5$ will be fixed below in the same way, but it will be necessary to take into account the shifts induced by the intramolecular couplings V_{ei}.

The half-widths γ_i vary around an average ~9 cm^{-1}, corresponding clearly to intramolecular vibrational processes, since the contribution of rotational multiple transitions and molecular inhomogeneity is $\Delta\nu_0/2=1.5$ cm^{-1}. The mode inhomogeneous half-width has been estimated to be ~5 cm^{-1} for the ν_1 and ν_4 modes, so that it represents clearly the major contribution to the peak A of $^{12}CF_3I$, or to the peak L of $^{13}CF_3I$. The large half-width of the peak A in $^{13}CF_3I$ reflects probably the underlying pres-

ence of secondary peaks, corresponding for example to the peaks d and e of $^{12}CF_3I$, which overlap with the main ν_1 peak: This is an effect of a strong but limited redistribution to close secondary resonances. At the extreme opposite, the peak e of $^{12}CF_3I$ is exceptionally narrow, $\gamma_e=2$ cm^{-1}. This value is close to the rotational and inhomogeneous contribution $\Delta\nu_0/2=1.5$ cm^{-1}, so that we must extract a corrected value $\bar{\gamma}_e$ using $\gamma_e^2=\bar{\gamma}_e^2+(\Delta\nu_0/2)^2$:

$$\bar{\gamma}_e\sim 1.3 \text{ cm}^{-1}\geqslant\gamma_{\text{diss}}. \tag{8}$$

The corrected value is indicated in Table II inside parentheses. A correction is unnecessary for the other half-widths. This small value provides an upper bound to the dissipative half-width γ_{diss}, very close to the estimate obtained for SF_6. The case of the ν_4 mode deserves a special comment because it is a degenerate mode ($g_4=2$) and we could expect an anharmonic splitting, according to Eq. (A2) with $G_{44}=4.35$ cm^{-1}. At $E=19\,000$ cm^{-1} we predict a spreading of the ν_4 mode over a range ± 20 cm^{-1}. For $^{13}CF_3I$, the ν_4 mode is entirely observed and splitted in two narrow peaks L and m. In Ref. 12, it has been suggested that m is the secondary resonance $2\nu_3+\nu_5$ which has a ground level value $\nu_i(0)=1109$ cm^{-1}. Then, we must accept that the low level anharmonic splitting cannot be extrapolated up to 19 000 cm^{-1} and that, for example, an effective constant $G_{44}(E)$ tends to zero at high levels.

The integrated oscillator strength $\bar{S}_i$ of each resonance is indicated in arbitrary unit (intensity$\times$cm^{-1}) in Table II, with the great uncertainty on the peak b, only guessed by its edges. From $\bar{S}_i$, an estimate of the coupling V_{ei} with the main closest resonance, can be made using a two levels approximations, and is indicated in Table II. There are mainly two groups of peaks: b for the two isotopes and c for $^{12}CF_3I$ have couplings of magnitude ~ 30 cm^{-1}, while d, e, and m have couplings of magnitude 5–10 cm^{-1}. The peak c of $^{13}CF_3I$ appears nevertheless in an intermediate range. It is tempting to assign the first group of resonances to the order $k=3$, and the second to the next order $k=4$, k being the number of vibrational quanta exchanged (Sec. II).

In Table II the parameter γ_i of each resonance corresponds actually to a half-width and it has been checked that it is dominated by mode inhomogeneity, or multiple transitions, or clusters of close resonances, in agreement with Eq. (6a). It is also interesting to explore the spectra of Refs. 10–12 in the minima between well separated resonances, to extract a parameter γ which is linked to intramolecular couplings out of resonance, according to Eq. (6b). This can be made at $\nu=1065$ cm^{-1} for $^{12}CF_3I$ and $\nu=1040$ cm^{-1} for $^{13}CF_3I$, in the minima between the ν_1 and ν_4 peaks. The identification between the experimental ratio $I(\nu)/\Sigma\bar{S}_i$ and its theoretical expression through Lorentzian functions gives $\gamma\sim 10$ cm^{-1} in the two cases. If we interpret this value by a secondary resonance spread over a width $2\Delta_I\sim 15$ cm^{-1} [Eq. (6b)], this gives an effective coupling $V_e\sim 7$ cm^{-1}, i.e., of the same magnitude as the previous second class of couplings assigned to the order $k=4$. The result is indicated at the end of Table II.

C. Assignment of the resonances at $E=19\,000$ cm^{-1}

In Refs. 10–12, the peaks c and e of $^{12}CF_3I$ were, respectively, assigned to the $\nu_2+\nu_3$ and $2\nu_5$ Fermi resonances, assuming that the order in their positions is unchanged from $E=0$ to $E=19\,000$ cm^{-1}. Peaks b and d were not considered because partly explored or too weak. In $^{13}CF_3I$, peak c was assigned to $\nu_2+\nu_3$, peak $e\equiv 2\nu_5$ was assumed not visible, because entangled in the broad peak $A\equiv\nu_1$, or on the contrary too far from it, peak b was not considered because partly explored, and peak m was assigned to the three frequency resonance $2\nu_3+\nu_5$ with the ν_4 peak.

The previous assignment presents several weaknesses, which are in fact mainly due to the identification of the peak e of $^{12}CF_3I$ with the $2\nu_5$ Fermi resonance. We can list all these weaknesses as follows.

The coupling of the peak e with ν_1 is 6 cm^{-1} at $E=19\,000$ cm^{-1} (Table II), while the $\nu_1/2\nu_5$ coupling increases from 2.6 cm^{-1} at $E=0$ cm^{-1}, to 12.5 cm^{-1} at $E=3200$ cm^{-1} (Table I). It is very unlikely that a diminution occurs in this coupling between $E=3200$ and 19 000 cm^{-1}.

In spite of its uncertainty the peak b can be explained by a coupling of a magnitude ~ 30 cm^{-1}, as for peak c. It is likely that these two similar couplings correspond to the same rank $k=3$, i.e., the resonances $2\nu_5$ and $\nu_2+\nu_3$, while all the other peaks (d,e,m), about fourfold smaller, correspond to the next rank $k=4$ (cf. the RQET model).

The linear anharmonic shift $-a_iE$ predicts the following order in the resonances at $E=19\,000$ cm^{-1}: $2\nu_5$ (928 cm^{-1}), $\nu_2+\nu_3$ (958 cm^{-1}), and ν_1 (977 cm^{-1}). A positive nonlinear shift must probably be added, as for the ν_4 mode, but we see that the order of the resonances is predicted to be reversed compared with the ground level order ($E=0$). The positive nonlinear shift must probably be considered as a correction to the main linear part, so that the order predicted by the linear part is a better assumption.

In Refs. 13–15, an isotopic selectivity ~ 1.3–1.5 has been reported in the dissociation of $^{12}CF_3I$ or $^{13}CF_3I$ sensitized by collisions with SF_6, this one being preexcited by IRMPA. This isotopic selectivity has found a natural explanation if a resonance of CF_3I at $E=19\,000$ cm^{-1} overlaps strongly with a resonance of SF_6 at $\langle E\rangle\sim 5000$ cm^{-1}, the overlapping being better for $^{13}CF_3I$ than for $^{12}CF_3I$. Through the dipole–dipole interaction, it is therefore possible to explain that the intermolecular energy transfer from SF_6 to CF_3I is higher for the $^{13}CF_3I$ species, which explains in turn a higher dissociation rate. The presence of a strong peak b, in close resonance with the ν_3 SF_6 mode, is therefore crucial to explain the previous effect. This one provides, conversely, a critical condition on the exact weight of the peak b in $^{12}CF_3I$ and $^{13}CF_3I$, and this will be used later.

All the previous weaknesses can be removed, at least qualitatively, if we accept the presence of the $2\nu_5$ Fermi resonance near $\nu=925$ cm^{-1}, where we guessed the presence of a peak b. The assignment of the peak c as the $\nu_2+\nu_3$ Fermi resonance remains perfectly justified. Peaks d and e of $^{12}CF_3I$ must be assigned to resonances of higher

TABLE III. Variations of the modelized $^{12}CF_3I$ and $^{13}CF_3I$ spectra at $E=19\,000$ cm^{-1} vs the coupling V_{Ac} between the ν_1 and $\nu_2+\nu_3$ resonances. Comparison with experimental data.

		$^{12}CF_3I$			$^{13}CF_3I$							
		ν_b ν_c ν_A (cm^{-1})	$R_{b/A}$		ν_b ν_c ν_A (cm^{-1})		$R_{b/A}$		$R_{c/A}$		$\alpha^T_{13/12}$	
V_{Ac} (cm^{-1})	V_{Ab} (cm^{-1})	Exp	Th	Exp	Th	Exp	Th	Exp	Th	Exp	Th	Exp
		925	0.023	>0.09 <0.27	927	~925	0.062	>0.25 <0.74	0.893	0.42		
27	12	975 1034			966 1019	985 1018					1.11	~1.35
30	27.5		0.171		920 967 1020		0.357		0.744		1.26	
32	31.5		0.279		917 968 1021		0.560		0.643		1.27	

order, (probably $k=4$). As discussed in Sec. III B, the peak m of $^{13}CF_3I$ can be interpreted as a secondary resonance of order $k=4$ (likely the $2\nu_3+\nu_5$ resonance). It is difficult to have a clear assignment of the other resonances of order $k=4$, i.e., of the form $\nu_i/\nu_j\pm\nu_k\pm\nu_l$, and this will not be attempted here.

We want now to make the new assignment more quantitative. We focus on the resonances of order $k=3$: $b\equiv 2\nu_5$ and $c\equiv\nu_2+\nu_3$, coupled to $A\equiv\nu_1$. The oscillator strengths of d and e are therefore grouped with that of A for $^{12}CF_3I$. We have five experimental data: the observed frequencies ν_A, ν_b, ν_c, and the two relative weights $R_{b/A}=\bar{S}_b/\bar{S}_A$ and $R_{c/A}=\bar{S}_c/\bar{S}_A$. We have five theoretical parameters: the three unperturbed frequencies $\bar{\nu}_A$, $\bar{\nu}_b$, $\bar{\nu}_c$, and the two effective couplings V_{Ab} and V_{Ac}. We assumed that the states $\bar{b}$ and $\bar{c}$ are prediagonalized and the remaining couplings are only with $\bar{A}$. This diagonalization problem has a well known solution, even for an arbitrary number of prediagonalized states.[30] In our case, there is a problem raised by the bad knowledge of the parameter $R_{b/A}$, due to the uncertainty about $\bar{S}_b$ (Table II). Then, we consider V_{Ac} as a free parameter and for each of its values, we determine the set $\bar{\nu}_A$, $\bar{\nu}_b$, $\bar{\nu}_c$, and V_{Ab} from the experimental $^{12}CF_3I$ data: ν_A, ν_b, ν_c, $R_{c/A}$. As indicated later, V_{Ab} is very sensitive to the choice of V_{Ac}, so that it is more suitable to choose V_{Ac} as the adjustable parameter.

The values of V_{Ac} are constrained in the following way. First, the predicted $R_{b/A}$ for the ^{12}C species must lie in the large possible range provided by $\bar{S}_b$ in Table II. Second, we can predict the corresponding $^{13}CF_3I$ spectrum, assuming that the isotopic shifts of the frequencies are the same at $E=19\,000$ cm^{-1} and $E=0$. Then $\bar{\nu}_A^{13}=\bar{\nu}_A^{12}-28$ cm^{-1}, $\bar{\nu}_b$ and $\bar{\nu}_c$ being practically unchanged. The couplings $V_{A/b}$, $V_{A/c}$ are also assumed unchanged. The predicted values can be compared to the experimental data of Table II for $^{13}CF_3I$.

Finally, we know from Refs. 13–15, that an isotopic selectivity $\alpha^D_{13/12}\sim 1.35$ has been obtained in the CF_3I dissociation rates, for the following conditions: pressures $P_A=P_{SF_6}=0.380$ Torr, $P_X=P_{CF_3I}=0.190$ Torr, fluence $\phi=1.00$ J/cm^2 exciting SF_6 by IRMPA at $\nu_L=944$ cm^{-1}. In these conditions, a quasiequilibrium is obtained during ~ 300 μs and the dissociation isotopic selectivity $\alpha^D_{13/12}$ can be related to a nearly identical isotopic selectivity $\alpha^T_{13/12}$ on the energy transfer:

$$\alpha^T_{13/12}=\frac{\langle\Delta E_{13}\rangle}{\langle\Delta E_{12}\rangle}, \tag{9}$$

where $\langle\Delta E_i\rangle$ is the average energy transferred per gas kinetic collision to the isotopic species $^iCF_3I$, this one being at $E=19\,000$ cm^{-1} (the selectivity on the dissociation rate depends only on the transfer on nearly dissociating molecules). The relation of Eq. (9) can be used assuming that $\langle\Delta E\rangle$ can be shared in two parts: one part $\langle\Delta E_{ns}\rangle$ concerning nonselective V-V or V-T transfers due to short range collisions between SF_6 and CF_3I, or CF_3I and CF_3I; and one part $\langle\Delta E_{dd}\rangle$ corresponding to a selective vibrational dipole–dipole interaction[13,15,31] between SF_6 and CF_3I. $\langle\Delta E_{ns}\rangle$ has been estimated[15] to be ~ -200 cm^{-1} in the previous conditions, while $\langle\Delta E_{dd}\rangle$ can be expressed through the overlapping integral I_{AX} between the IR active oscillator strengths of A=SF_6 and X=CF_3I.

The isotopic effect, briefly presented here, will be analyzed thoroughly elsewhere. From Eq. (9) and using the computed weights of the peak b of $^{12}CF_3I$ and $^{13}CF_3I$, we can obtain the overlapping integral I_{AX} with the ν_3 SF_6 mode and therefore a theoretical estimate of $\alpha^T_{13/12}\sim\alpha^D_{13/12}$, for each value of V_{Ac}.

The results of the computations are presented in Table III for three values of the free parameter V_{Ac}, and compared with the experimental values. We note first the extreme sensitivity of several parameters (V_{Ab},$R_{b/A}$,$\alpha^T_{13/12}$) to small variations of V_{Ac}. This fact permits an accurate determination of this parameter. The value 27 cm^{-1} is excluded by a too low result for $R_{b/A}$, for the two isotopes. It is more difficult to decide between the values 30 or 32

TABLE IV. Parameters of the anharmonic shifts of $^{12}CF_3I$ at $E=19\,000$ cm^{-1} for $V_{Ac}=30$ cm^{-1}.

Res	ν_i (obs.) (cm^{-1})	$\bar{\nu}_i$ (cm^{-1})	Δ_L (cm^{-1})	Δ_{NL} (cm^{-1})	b_i (10^{-8} cm)
ν_1	1033	1004	−99	+28	7.76
$\nu_2+\nu_3$	975	993	−72	+35	9.70
$2\nu_5$	~925	937	−152	~+9	~2.49
ν_4	~1100	~1100	−123	~+36	~9.97

cm^{-1}. For 32 cm^{-1}, $R_{b/A}$ is slightly outside the experimental possible range for $^{12}CF_3I$, but the $R_{c/A}$ value is better for $^{13}CF_3I$. The best choice seems to be $V_{Ac}=30$ cm^{-1} and, therefore, $V_{Ab}=27.5$ cm^{-1}. Obviously, ν_b, ν_c, ν_A, and $R_{c/A}$ are perfectly reproduced for $^{12}CF_3I$, since the parameters $\bar{\nu}_b$, $\bar{\nu}_c$, $\bar{\nu}_A$, and V_{Ab} are chosen for this purpose. $R_{b/A}$ is also in very good agreement with the most likely values, either for $^{12}CF_3I$ or $^{13}CF_3I$. The positions ν_A and ν_c for $^{13}CF_3I$ are very well predicted, but this is the case for the three values V_{Ac}. The isotopic selectivity $\alpha^T_{13/12}$ has the correct magnitude. The single weakness lies in the characteristics of the peak c in $^{13}CF_3I$. Its predicted position (967 cm^{-1}) is shifted −18 cm^{-1} from its experimental value (985 cm^{-1}) and its weight ($R_{c/A}$) would be correctly reproduced with $V_{Ac}\sim 35$ cm^{-1}, but $R_{b/A}$ would be unrealistic. The result of the computed spectra, for $V_{Ac}=30$ cm^{-1}, is plotted in the lower parts of Fig. 2 and is in satisfactory agreement with experiment. The ν_4 peak is represented with the weight derived from the ratio K_4/K_1 of the ground level (Table I). The presence of peaks d and e in the $^{12}CF_3I$ spectrum could be easily introduced with the $\bar{\nu}_i$ and V_{1i} *ad hoc* parameters.

The discrepancy concerning peak c in $^{13}CF_3I$ deserves a special comment, because the −18 cm^{-1} shift of the position is unaccountable within a three level model with realistic isotopic shifts: as peak A has a frequency $\bar{\nu}_A$ shifted of ~ -28 cm^{-1} from ^{12}C to ^{13}C, peak c must be repelled to a lower frequency (from 975 to 966 cm^{-1} in our model). The experimental shift is the opposite: from 975–985 cm^{-1}. The single explanation we see to this peculiar fact lies in the role of the peak d which can repel peak c to high frequencies. The resonance $d=\nu_1-\nu_3+\nu_6$ which has the same isotopic shift as the ν_1 mode and detuned of it by −25 cm^{-1} could explain this feature.

We can finally list the unperturbed frequencies $\bar{\nu}_i$ of the resonances ν_1, $\nu_2+\nu_3$, $2\nu_5$, and ν_4 at $E=19\,000$ cm^{-1}, obtained for $V_{Ac}=30$ cm^{-1}, and compute the linear anharmonic shift Δ_L and the nonlinear part Δ_{NL} which gives the coefficient b_i in Eq. (7). The results are reported in Table IV for $^{12}CF_3I$. The values of Table IV call for a few comments. The small observed anharmonic shift of the ν_1 mode relative to the ground level frequency (−42 cm^{-1}) is due for a great part to the strong repulsion between the ν_1 and $\nu_2+\nu_3$ resonances for $V_{Ac}=30$ cm^{-1}. The unperturbed frequency $\bar{\nu}_1$ gives a greater anharmonic shift −71 cm^{-1}. This one is shared in a dominant linear part −99 cm^{-1} and a positive nonlinear part, non-negligible but smaller: +28 cm^{-1}. In fact all nonlinear parts appear positive and smaller than the linear part. The $2\nu_5$ has a particularly small nonlinear part. The determination of the b_i coefficients permits now the prediction of $\bar{\nu}_i(E)$ from 0 to 19 000 cm^{-1}, for all the main resonances.

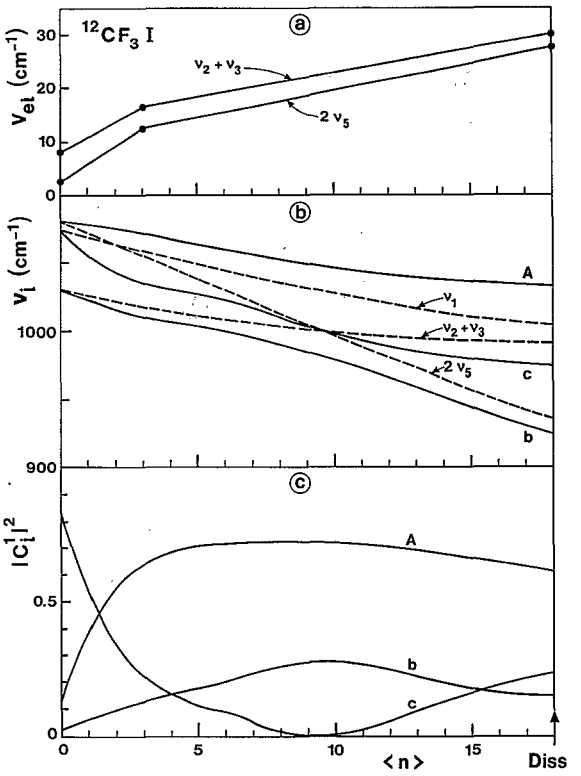

FIG. 3. Computed positions and weights of the resonances A, b, c vs energy, expressed with the number n of photons $h\nu_L=1072$ cm^{-1}. (a) Linear interpolation of the couplings V_{ei} between the ν_1 line and the $\nu_2+\nu_3$ and $2\nu_5$ lines; (b) unperturbed frequencies $\bar{\nu}_i$ (dashed lines), and resulting frequencies ν_i (solid lines) of the resonances A, b, c vs n; (c) weight $|C_i^1|^2$ of the ν_1 mode in each resonance A, b, c, vs n.

D. Interpolation of the resonance characteristics from $E=0$ to 19 000 cm^{-1}

In view of the analysis of CF_3I IRMPA data from $E=0$ to 19 000 cm^{-1}, in Sec. IV, we are now in position to interpolate with good confidence the resonances ν_1, $\nu_2+\nu_3$, $2\nu_5$, and ν_4 in the same energy range, either for their location or their weight. For this purpose, we interpolate the unperturbed frequencies $\bar{\nu}_i$ using Eq. (7), with the coefficients a_i in Table I, and the coefficients b_i in Table IV. It is then necessary to compute the redistribution of the ν_1 mode toward the $\alpha=\nu_2+\nu_3$ and $\beta=2\nu_5$ Fermi resonances, due to the respective couplings $V_{1\alpha}$ and $V_{1\beta}$. We use a linear interpolation from $E=0$ to $E=3200$ cm^{-1}; $V_{1\alpha}$ increases from 8.2 to 16.5 cm^{-1}, and $V_{1\beta}$ from 2.6 to 12.5 cm^{-1} (Table I), and a second linear interpolation from $E=3200$ to 19 000 cm^{-1}; $V_{1\alpha}$ increases from 16.5 to 30 cm^{-1}; and $V_{1\beta}$ from 12.5 to 27.5 cm^{-1}. This is represented in Fig. 3(a), using the energy unit of one photon $h\nu_L=1072$ cm^{-1}. With these coefficients it is easy to solve the three-level diagonalization problem ν_A, ν_b, ν_c for each E as in Sec. III C. The positions $\nu_i(E)$ are indicated in Fig. 3(b) with solid lines, the resonances being labeled A, b, c continuously, in agreement with the previous labeling at

$E=19\,000\ cm^{-1}$. The unperturbed positions $\bar{\nu}_i(E)$ are indicated by dashed lines. The $\bar{\nu}_1$ and $2\bar{\nu}_5$ lines cross near $n=2$, and the $\bar{\nu}_2+\bar{\nu}_3$ and $2\bar{\nu}_5$ lines near $n=10$. In Fig. 3(c), the weight $|C_i^1|^2$ of the ν_1 mode in each resonance A, b, c is plotted vs n, giving the total oscillator strength of each resonance vs energy. Owing to the crossing of the unperturbed resonances, the dominant part of each resonance varies vs n. For example, A is mainly the $2\nu_5$ line for $n<2$, while it is dominated by ν_1 above; the resonance b is dominated by $\nu_2+\nu_3$ for $n<10$, and by $2\nu_5$ above. Note that the intermediate resonance c has a weight $|C_c^1|^2=0$ at the crossing between $\nu_2+\nu_3$ and $2\nu_5$ near $n=10$.

IV. EXTRACTION OF THE LORENTZIAN PARAMETER γ FROM IRMPA DATA

In Ref. 16, the kinetic equations describing the IRMPA and IRMPD processes were solved for CF_3I, using a Lorentzian description of the absorption coefficients. Only the ν_1 mode was taken into account. The resonance frequency $\nu_1(E)$ was assumed linearly shifted vs energy, with an adjustable coefficient a_1. The half-width $\gamma_1(n)$ was assumed to vary vs the number n of photons absorbed ($E=nh\nu_L$, with $\nu_L=1075\ cm^{-1}$), according to the law

$$\gamma_1(n)=V_1[n^{3/2}+(n+1)^{3/2}], \tag{10}$$

where V_1 was the second adjustable parameter. The dependence on n in Eq. (10) was justified by the assumed dominant role of three frequency Fermi resonances in the redistribution process, i.e., of terms of the form $V_{1ij}x_1x_ix_j$. The intramolecular couplings $|\langle a|V|b\rangle|$ are therefore roughly proportional to $n^{3/2}$ in the initial state, and $(n+1)^{3/2}$ in the final state. The experimental data was the dissociation yield $\beta(\langle n\rangle)$, and a_1 and V_1 were chosen to give the best fit. The result is $a_1=3.53\times10^{-3}$, $V_1=0.73\ cm^{-1}$. We can note that the result for a_1 is a good average between the coefficient a_1 valid for the low levels, $a_1=5.2\times10^{-3}$ (Table I), and the effective coefficient valid at $E=19\,000\ cm^{-1}$, 2.21×10^{-3} (see Table IV; $\nu_1=1033\ cm^{-1}$). From the coefficient V_1 we can compute the curve $\gamma_1(n)$ which is plotted in Fig. 4 and indicated as "Diss ν_1." Near the dissociation limit $E\simeq19\,000\ cm^{-1}$, the prediction is $116\ cm^{-1}$, in serious contradiction with the observed half-widths of the resonances (Table II), which are at least 1 order of magnitude smaller. We want to analyze this discrepancy and restore a unified description of CF_3I QC states.

Before a quantitative study of the problem, several remarks can be made on the extraction of γ in Ref. 16. First, the dependence on n in Eq. (10) is poorly justified. It was shown later[17–19,32–34] that, for three frequency resonances, the dependence is indeed $\gamma(n)\propto n$, as it was also derived in the context of phonons three decades ago.[35] Moreover, as it was shown for SF_6 in Refs. 1 and 3, three frequency resonances produce more likely perturbative or limited redistribution on well isolated resonances, while the smooth redistribution is linked to higher orders. In these works, it was also remarked that the energy dependence of a coupling of rank k is not accounted for by a Taylor expansion of the potential, as it is usually assumed. Therefore, any

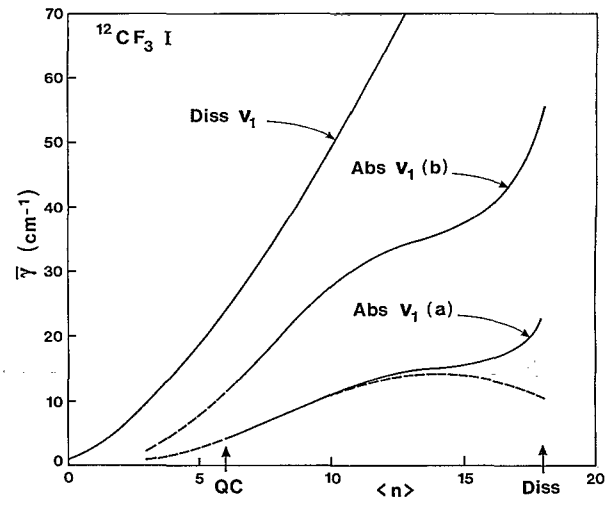

FIG. 4. Extraction of the Lorentzian parameter $\bar{\gamma}$ of $^{12}CF_3I$ vs the number $\langle n\rangle$ of photons $h\nu_L=1072\ cm^{-1}$ absorbed by IRMPE. In the curve Diss ν_1, $\bar{\gamma}$ is extracted from IRMPD data (reproduced from Ref. 16). In the curve Abs ν_1(a), $\bar{\gamma}$ is extracted from IRMPA data with a mode ν_1 having the same linear anharmonic shift as in Ref. 16. The dashed part is not corrected from the dissociation. In the curve Abs $\nu_1(b)$, $\bar{\gamma}$ is extracted from IRMPA data with a mode ν_1 having the same linear anharmonic shift as in the low energy levels.

hypothesis about the energy dependence of γ is questionable. Second, while it was shown in Ref. 3 that IRMPA data are very useful to extract a parameter γ, at least for SF_6, we think that IRMPD data are much more critical. The reasons are obvious: IRMPD data depend on the exact high energy tail shape of the distribution ($E\geqslant E_d$) with a high sensitivity; moreover, the dissociation yield depends on post pulse collisional processes or secondary chemical reactions, such as recombinations, over several tens microseconds, which were not taken into account in Ref. 16, and are difficult to modelize properly. Finally, the description of the cross section using a pure ν_1 mode appears as a poor approximation, knowing the experimental spectrum at $E=19\,000\ cm^{-1}$, which shows several other important resonances and particularly the ν_4 peak, close to the absorption frequency $\nu_L\sim1075\ cm^{-1}$ at this energy (Fig. 2).

From the previous remarks, we try to extract the parameter γ from IRMPA data. The curve $\gamma(E)$ will be extracted from the function $\langle n\rangle=f(\phi,\nu_L)$, were ϕ is the exciting laser fluence (J/cm^2) at the frequency ν_L. Then, no energy dependence of γ is assumed *a priori*, but in exchange, we need an accurate description of the position and weight of the different main resonances, provided by the results of Sec. III. The relation between the function $f(\phi,\nu_L)$ and the state to state absorption rates $Z_{n\to n+1}$ has been derived in Ref. 3 and we recall here the important results. We consider only the molecules above the QC threshold, which form the fraction q excited in the QC. From the experimental value $\langle n\rangle$, we can therefore derive the average level $\langle n_q\rangle$ reached by molecules excited in the QC. In the case of $^{12}CF_3I$, $\langle n\rangle$ and q can be found in Refs. 6–8. The useful data is the differential cross section

$$\sigma_d\langle n_q\rangle = h\nu_L d\langle n_q\rangle/d\phi \tag{11}$$

which can be related to the vibrational distribution and the absorption rates $Z_{n\to n+1}$. This one can be written (Fermi golden rule) as

$$Z_{n\to n+1} = I(t)\,U_{n\to n+1}. \tag{12}$$

It is possible to write the differential cross section as an average of the absorption rates over a distribution G. We restrict all quantities to the QC and omit the index q in the expression:

$$\frac{d\langle n\rangle}{d\phi} = Q\bar{U}(1-\bar{a}), \tag{13a}$$

with

$$\frac{1}{\bar{U}} = \left\langle \frac{1}{U_{n\to n+1}} \right\rangle_G . \tag{13b}$$

The factor Q depends on the dissociation of the molecule. Its value is 1 if the dissociation can be neglected and we will specify it with more details below. The main factor is the average $\bar{U}$ over the distribution G. It can be noted that the average uses the inverse of $U_{n\to n+1}$ ($\propto Z_{n\to n+1}$). This means that the high peaks in the absorption rates play a secondary role in the differential cross section, the physical reason being that in a multistep process, the slowest steps enforce the kinetics. An approximation to the distribution G, of a Gaussian form, is indicated in Appendix B vs the density of states $\rho(n)$, for a given average number of photons absorbed $\langle n\rangle$. The parameter $\bar{a}<1$ is also indicated. As the expression of the differential cross section involves an average, it is not too much sensitive to the exact distribution used. This relatively weak sensitivity was checked in a preliminary work on SF_6,[36] and it is the basic reason for the superiority of an extraction of γ from IRMPA data, instead of IRMPD data.

We finally need an expression for $U_{n\to n+1}$. For this purpose, we use the quasi-Lorentzian formalism for each resonance i

$$U_{n\to n+1} = \sum_i U^{(i)}_{n\to n+1}, \tag{14a}$$

$$U^{(i)}_{n\to n+1} = K_i(\bar{\nu}_{i\alpha}+1)\,\frac{1}{\pi}\,\frac{\gamma_i}{\Delta E_i^2+\gamma_i^2}, \tag{14b}$$

with

$$\Delta E_i = h\nu_i(E) - h\nu_L. \tag{14c}$$

K_i is the integrated cross section of the resonance i (cf. Table I). $\bar{\nu}_{i\alpha}(E)$ is the average number of quanta in one coordinate α of the main resonance (ν_1 or ν_4) responsible for the oscillator strength in i. $\gamma_i(E\to E+h\nu_L)\equiv\gamma_i(E)$ depends generally on E and is the unknown function we want to extract. If we have several resonances, it is not possible to derive the different functions $\gamma_i(E)$ from a unique data $\langle n\rangle = f(\phi,\nu_L)$ because ν_L is fixed by the low levels excitation and cannot be varied significantly. Then we make the hypothesis of a single function $\gamma_i=\gamma^{(0)}(E)$ whatever i. The rigorous extraction of $\gamma^{(0)}(E)$ would be a cumbersome problem needing trial functions and iterations. It is much more transparent to proceed in a different way: we fix a value $\gamma_i(E)=\bar{\gamma}$ in Eqs. (13) and (14), so that we compute a value $\bar{\gamma}(\langle n\rangle)$ which is a double average of the values $\gamma_i(n)$ over the different resonances i, and over the distribution G.

In the foregoing, we have not taken into account the dissociation, which is in fact negligible in CF_3I for a value of $\langle E\rangle$ up to $\sim$75% of the dissociation threshold $E\simeq 19\,000$ cm^{-1} ($n=18$). However, it is no more the case at $E\sim 19\,000$ cm^{-1} (Fig. 2). In Ref. 3, we proposed a correction. We assume that the dissociation produces a cutoff in the distribution G at a critical level n_c such that the dissociation rate K_d checks

$$K_d(n_c)\sim Z(n_c\to n_c+1). \tag{15}$$

In typical experiments, with 100 ns pulses, we get $K_d(n_c)\sim 10^{+9}$ Hz. The RRKM curves $K_d(E,J)$ have been reported in Ref. 37 for CF_3I. For $J\sim 50$, the critical level is near $E_c\sim 21\,000$ cm^{-1} ($n_c=19.6$). The value $Q<1$ is derived according to the expressions in Appendix B.

We apply this general procedure to the $^{12}CF_3I$ IRMPA using the data of Refs. 6–8 at the frequency $\nu_L=1072$ cm^{-1}. The experimental differential cross section for QC states ($n\geqslant 6$) can be fitted by the function.

$$\sigma_d(\langle n_q\rangle) = (46.5-2.2\langle n_q\rangle)10^{-20}\ \text{cm}^2. \tag{16}$$

The formula is valid up to the dissociation limit $n_d\sim 18$. It can be checked that $\sigma_d(n)\to 0$ for $n\simeq 21$. This is in agreement with the fact that the critical value n_c, estimated earlier, is the maximum possible absorption (see Appendix B). The coefficients K_1 and K_4 of the ν_1 and ν_4 modes are indicated in Table I. The positions of the resonances are computed with the coefficients $\nu_i(0)$ and a_i (Table I), b_i (Table IV), and if necessary with the diagonalization of coupled resonances (Sec. III D). In this last case, the weight of each resonance is also computed. Finally, the IRMPA data are obtained at a rotational temperature $T_{\text{rot}}\sim 300$ K, so that the rotational spreading is not negligible, particularly near resonance and in the low levels. Then, using the rotational coefficients A and B (Sec. III A), the mode ν_1 and its satellites $2\nu_5$ and $\nu_2+\nu_3$ are modelized by three branches at 0, ± 5 cm^{-1}, each one with a weight $\frac{1}{3}$, and the ν_4 branch by two branches ± 8 cm^{-1} with a weight $\frac{1}{2}$. This last modelization can also reproduce roughly the anharmonic splitting of the ν_4 mode (see Sec. III B). In fact, the modelization of the multiple transitions is not critical in two cases: (a) out of resonance or (b) inside a broad multiplet of resonances. The single critical case corresponds to an excitation inside a multiplet of well separated lines. This last case will not be encountered in the QC, i.e., for $n\geqslant 6$, so that the exact spreading of each resonance in a multiplet is not critical and the previous representation of the rotational splitting will be considered as a sufficient modelization.

We have first extracted the parameter $\bar{\gamma}$ with the same model as in Ref. 16, but using IRMPA instead of IRMPD data. The single ν_1 resonance is taken into account with the same linear anharmonic shift parameter $a_1=3.53\times 10^{-3}$.

The result is reported in Fig. 4 and indicated as Abs $\nu_1(a)$. The values obtained are about fivefold smaller than those derived from IRMPD data. Near the dissociation limit ($n=18$), $\bar{\gamma}\sim 22\ \mathrm{cm}^{-1}$ which is greater than the experimental values detailed in Sec. III but are in much more reasonable agreement. This fact shows the superiority of an extraction of γ from IRMPA data, the reason being explained at the beginning of this section. The dashed curve for $n\geqslant 12$ corresponds to data uncorrected from the dissociation. It is clear that the correction is not negligible for $n\geqslant 15$, and reaches a factor ~ 2 at $n=18$. The correction factor is nearly independent on the absorption model, and the uncorrected values are not reported for the next curves. The curve Abs $\nu_1(a)$, as well as the next curves, are plotted with dashed lines for $n\leqslant 6$, since the modelization of the multiplet becomes questionable, and the absorption process is coherent. It is nevertheless interesting to note that the IRMPA cross sections *could* be explained, near $n\sim 3$, by Lorentzian distributions of the oscillator strength with half-widths $\gamma\sim 1\ \mathrm{cm}^{-1}$.

The use of a parameter $a_1=3.53\times 10^{-3}$ is only dictated by the comparison with IRMPD data. Without this work, and in the absence of any other data, the most natural choice for a_1 would be that of low energy levels, i.e., $a_1=5.2\times 10^{-3}$ (Table I). The extraction of $\bar{\gamma}$ has been made again, with the single resonance ν_1 and this last value of a_1. The result corresponds to the curve Abs $\nu_1(b)$. The value of $\bar{\gamma}$ extracted from Eqs. (13) and (14) is mainly proportional to the square detuning $|\Delta\nu|^2$ and, therefore to a_1^2, out of resonance. This fact explained why the result of the curve Abs $\nu_1(b)$ is about 2.5 that of the curve Abs $\nu_1(a)$. The comparison shows the sensitivity of the extraction to a good knowledge of the main resonances. Near the dissociation limit, the value of the curve Abs $\nu_1(b)$ reaches $\bar{\gamma}\sim 55\ \mathrm{cm}^{-1}$ and is clearly ruled out by experiments.

As we have seen in Sec. III, the strong anharmonicity of the mode ν_4 makes this resonance closer of the exciting frequency at high energy. We can estimate its role in the IRMPA process using the linear shift $a_4=6.5\times 10^{-3}$ (Table I), assuming again we have no other data to refine the description. The result of this model, using the two resonances ν_1 and ν_4 and the linear shifts of Table I, is plotted in Fig. 5 and corresponds to the curve Abs $\nu_1+\nu_4(b)$. The beginning of the previous curve Abs $\nu_1(b)$ has also been plotted for comparison. Note the ordinate scale is different from that of Fig. 4. It is striking that the presence of the ν_4 resonance is important since the beginning of the QC. The value predicted at $n=18$ is $\bar{\gamma}\sim 3\ \mathrm{cm}^{-1}$, i.e., nearly twentyfold smaller than in the model taking only into account the ν_1 mode. This is due to the fact that, with a purely linear anharmonic shift, the ν_4 mode is predicted to be in full resonance with the excitation near the dissociation limit. The result shows the importance to check off all the main resonances involved in the IRMPA process, to interpret it correctly. The shape of the curve presents a maximum $\bar{\gamma}\sim 12\ \mathrm{cm}^{-1}$ near $n=9$ and decreases down to the aforementioned value $\bar{\gamma}=3\ \mathrm{cm}^{-1}$. This can be considered poorly justified physically, but the decrease above $n=9$ could reflect, for example, the more and more important

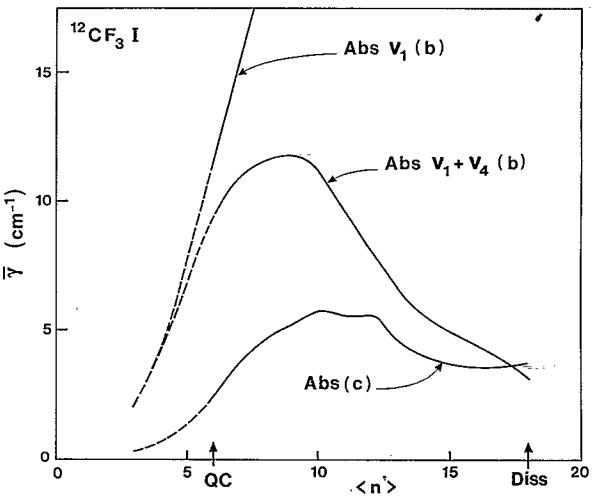

FIG. 5. Extraction of $\bar{\gamma}$ as in Fig. 4. Note the different scale. The curve Abs $\nu_1(b)$ reproduces that of Fig. 4 for comparison. In the curve Abs $\nu_1+\nu_4$(b), $\bar{\gamma}$ is extracted from IRMPA data taking into account the two modes ν_1 and ν_4 with the same linear anharmonic shifts as in the low energy levels. In the curve Abs(c), $\bar{\gamma}$ is extracted from IRMPA data, taking into account the four resonances ν_1, ν_4, $\nu_2+\nu_3$, $2\nu_5$ with the positions and weights obtained in Sec. III D.

role of the ν_4 mode with a parameter $\gamma_4\sim 3\ \mathrm{cm}^{-1}$, while γ_1 would be $\sim 15\ \mathrm{cm}^{-1}$.

Finally, the description of the resonances in Sec. III D using linear and quadratic anharmonic shifts and coupled $\nu_1/\nu_2+\nu_3/2\nu_5$ resonances as well as the ν_4 line, has been used to extract the most likely parameter $\bar{\gamma}$. This extraction is obviously possible only because a spectrum is available and properly interpreted at $E=19\,000\ \mathrm{cm}^{-1}$. The result is the curve Abs (c). The curve begins at a much slower rate and is only $\bar{\gamma}\sim 2.5\ \mathrm{cm}^{-1}$ at the beginning of the QC. It increases up to $\bar{\gamma}\sim 5$–$6\ \mathrm{cm}^{-1}$ near $n=10$ and decreases moderately above, to reach a value $\bar{\gamma}\sim 4\ \mathrm{cm}^{-1}$ near the dissociation limit. This shape is undoubtly much more likely than the curve Abs $\nu_1+\nu_4(b)$, and the value at $n=18$ is in very good agreement with the magnitude of the parameters γ observed at $E=19\,000\ \mathrm{cm}^{-1}$, either when they represent half-widths or out of resonance redistributed fluorescence (Table II). We can therefore consider that the present description removes all contradictions and that the CF_3I IRMPA process in the QC is correctly understood.

We can also comment the extreme opposite of the curve, i.e., the values obtained below the QC onset. It could be considered that these values are meaningless but this is not always the case. It was shown in Ref. 9, that for laser linewidths $\Delta\nu_L\geqslant 0.1\ \mathrm{cm}^{-1}$, an enhancement $\Delta\sigma_d\sim 20\times 10^{-20}\ \mathrm{cm}^2$ of the absorption cross section occurs, the characteristics of which suggest that a set of weak lines with a spacing $\epsilon\sim 0.1\ \mathrm{cm}^{-1}$ exists and becomes involved in the absorption process. When $\Delta\nu_L\geqslant\epsilon$, these weak lines act as a QC and can be treated in the previous incoherent formalism.

We can now discuss the accuracy of the previous extraction of $\bar{\gamma}\cdot\bar{\gamma}$ is roughly proportional to $\sigma_d\Delta\nu^2$. The ac-

curacy about $\Delta\nu$ is probably $\sim 10\%$, so that the resulting accuracy on $\bar{\gamma}$ is $\sim 20\%$, which does not change the magnitude. The error on $\sigma_d(\langle n_q\rangle)$, the differential cross section of molecules above the QC onset, is more doubtful as revealed by the recent work of Ref. 38. In this work, photoionization of $I(^2P_{3/2})$ allows to measure fractions f_0, f_a, f_b, f_c of molecules in the discrete levels, between the QC onset and the dissociation threshold, around the dissociation threshold within 1000 cm^{-1}, and above this range. A model of population equations leads to a reconstruction of the distribution. The existence of a bimodal distribution is confirmed and justifies the need to consider only molecules excited in the QC (the fraction f_q of Refs. 6–8). Unfortunately, the results of Ref. 38 and those, used in this work, of Refs. 6–8, are significantly different. At 0.5 J/cm^2, $f_q \sim 50\%$ and $\langle n_q\rangle \sim 12.5$ in Refs. 6–8, while $f_q \sim 70\%$ and $\langle n_q\rangle \sim 17$ in Ref. 38. This last value $\langle n_q\rangle$ is particularly awkward, because it means that the correction of dissociation is necessary even at 0.5 J/cm^2. The average value of σ_d in the QC for Ref. 38 is therefore at least twice that of Refs. 6–8, resulting in a doubling of $\bar{\gamma}$. It must be underlined that Refs. 6–8 provide directly the quantity $\langle n_q\rangle$, while Ref. 38 gives only four fractions of the distribution, the fraction f_a concerning a very broad range, so that we think the results of Refs. 6–8 are more relevant for our purpose. A doubling of $\bar{\gamma}$, would give values ~ 10 cm^{-1} near the dissociation threshold, which are acceptable, although a little to high, compared with the experimental spectroscopy (cf. Table II). This shows that it is not possible to obtain presently more than an agreement of magnitude on the parameter $\bar{\gamma}$. Perhaps, the different data of Refs. 6–8 and 38 could be reconciled, taking into account in the population equations the fact that $Z_{n\to n+1}$ increases strongly near the dissociation threshold, owing to the closer and closer presence of the ν_4 line, shifted by anharmonicity. This effect can overpopulate dissociation levels, the average $\langle n_q\rangle$ remaining near 12.5.

A useful remark for Sec. V can be made about the curve Abs (c) in Fig. 5: The energy dependence is roughly flat above $n=10$. As it will be quantitatively justified in Sec. V, $\bar{\gamma}$ is dominated by the highest couplings which are of rank $k=4$, since the rank $k=3$ has been treated separately. Then we get the puzzling result that couplings of rank $k=3$ are increasing with E, roughly as $E^{1/2}$, while couplings of rank $k=4$ have a much weaker energy variation.

V. MODELIZATION OF THE COUPLINGS HIERARCHY

We can now analyze the intramolecular redistribution scheme using the ideas of the RQET formalism (see the end of Sec. II) in which each rank k of couplings is associated with a magnitude of matrix elements V_k, exponentially decreasing with k:

$$V_k = V_0/a^k, \tag{17}$$

where k is interpreted as the number of vibrational quanta exchanged. We therefore need to fix two parameters, V_3 and V_4, to obtain the modelization of the couplings. In the more general case, these parameters V_0 and a depend on the initial state considered, or at least on the total energy of this initial state. The second important quantity is the density ρ_k of final states coupled to the initial state by matrix elements of order k. This quantity has two applications: It serves to compute the contribution $\gamma_k = \pi\rho_k V_k^2$ [Eq. (1a)], as was made in RQET,[21–25] but also to compute the parameter $\pi\rho_k V_k$ determining if the redistribution is perturbative or dissipative [Eq. (2)]. This second application was not considered in RQET, but was applied successfully to SF_6 in Ref. 3 to obtain either the dissipative linewidth γ_{diss} or the QC threshold, comparing very well with the results of picosecond experiments[4,5] or Raman monitoring.[6–8] The determination of ρ_k is a counting problem which can be solved knowing only the molecular frequencies, a harmonic approximation being generally sufficient. Our purpose is to extract the main parameters determining the IVR and not to obtain accurate results. Then, we shall use approximate expressions of ρ_k, valid in two typical situations. The first corresponds to a separable state at sufficiently high energy, with an equipartition of energy among the modes; the second corresponds to an overtone state of a pumped mode ν_a. The respective expressions of ρ_k, obtained in Ref. 3, are recalled in Appendix C.

In the first case, we consider a separable state of energy E, representative of a statistically redistributed QC state, i.e., such that in each mode i, $E_i = v_i h\nu_i \sim E/s$, s being the number of coordinates (for the sake of simplicity, we assume here that the modes are not degenerate). To obtain the approximate expression ρ_k, of Appendix C, it is necessary to admit that $v_i > 1$. We define an average frequency $\bar{\nu}$, and also the total number of quanta $v \sim E/h\bar{\nu}$. The previous condition is therefore $E > sh\bar{\nu}$. For CF_3I, $sh\bar{\nu} = 6080$ cm^{-1}, so that the condition is fulfilled above the experimental QC onset. We have chosen to study the state at $n=10$ photons $h\nu_L = 1072$ cm^{-1} absorbed. The expression ρ_k scales as $1/\bar{\nu}$ but it is necessary to fix an adjustable parameter F, the magnitude of which is ~ 1, F taking into account the frequencies dispersion and symmetry restrictions. This parameter F is determined from the experimental value ρ_3. In Ref. 27, five Fermi resonances of the type $\nu_i + \nu_j$ are observed between 788 and 1281 cm^{-1}, which gives $\rho_3 = 8.14 \times 10^{-3}$ cm.

A second difficulty was analyzed in Ref. 3. For the lowest orders $k=3,4$, owing to the degeneracy of several modes, what is seen in spectra are groups of quasidegenerate levels corresponding to an effective number of degrees of freedom s_e, which is $s_e = 6$ for CF_3I. The full number of degrees of freedom is $s_f = 9$ for CF_3I. For $k=3$, the different groups of levels are clearly separated and we observe in spectra a density of coupled states ρ_k^e. Using $\rho_3^e = 8.14 \times 10^{-3}$ cm and $s = s_e = 6$ in the expression of Appendix C, we obtain the scaling frequency $2F\bar{\nu} = 2580$ cm^{-1}, i.e., $F \sim 1.9$, which allows the computation of all values ρ_k. We get for example, $\rho_4^e = 3.66 \times 10^{-2}$ cm with $s = s_e = 6$. The problem of choosing s will be treated later

Restricting again to the lowest orders, for which $s = s_e$ must be used, we can now determine the parameters V_3 and V_4, and therefore a, of the couplings model, from experimental data. These couplings concern groups of degenerate levels and we note these parameters V_3^e, V_4^e, a_e. At

$E=19\,000\ cm^{-1}$, the results in Table II and the lines assignment in Sec. III C fix an estimate for these parameters: Peaks b and c correspond to the rank $k=3$, since they are assigned, respectively, to the $2\nu_5$ and $\nu_2+\nu_3$ lines. Then $V_3^e\sim 28\ cm^{-1}$ [see the exact values in Fig. 3(a)]. Peaks d, e, m and the oscillator strength near the minima at 1065 or 1040 cm^{-1} are assigned to the next order $k=4$, so that $V_4^e\sim 7\ cm^{-1}$ (see Table II). Then $a_e\sim 4.0$. These values are similar to those obtained for SF_6 near $E=17\,000\ cm^{-1}$: $V_3^e\sim 16\ cm^{-1}$; $V_4^e\sim 5\ cm^{-1}$; $a_e\sim 3.2$.

It is not possible to have a direct information on V_3^e and V_4^e at an intermediate energy. At $n=10$, the interpolation in Fig. 3(a) gives $V_3^e\sim 21\ cm^{-1}$. A second constraint can be given by the value $\bar{\gamma}$ obtained from IRMPA data. At $n=10$, we get $\bar{\gamma}\sim 5.5\ cm^{-1}$. From the analysis of Sec. II, $\bar{\gamma}$ can be interpreted as due to the out of resonance redistributed oscillator strength, through orders $k\geqslant 4$, since the order $k=3$ gives well isolated resonances treated separately. Then, we identify

$$\bar{\gamma}\simeq\sum_{k\geqslant 4}\gamma_k. \tag{18}$$

As shown in Ref. 3, the value γ_k is independent on the computation through groups of levels or individual levels:

$$\gamma_k^e=\gamma_k^f. \tag{19}$$

Then, we can express $\bar{\gamma}$ using $V_3^e=21\ cm^{-1}$, the expressions ρ_k^e, and an adjustable parameter a_e. $\bar{\gamma}=5.5\ cm^{-1}$ gives $a_e=3.75$ at $n=10$. This determines completely the model at $n=10$ ($E\simeq 10\,700\ cm^{-1}$). We observe that a_e does not vary very much from $n=10$ to $n=18$ (from 3.75 to 4.0). This weak dependence of a_e vs E was also observed for SF_6 and will be commented later.

Fixing again $s=s_e=6$, we can now compute at $n=10$ the parameters γ_k and $\pi\rho_k^eV_k^e$ vs k. The curves are plotted in Fig. 6(a) in semilogarithmic coordinates. $\pi\rho_k^eV_k^e$ corresponds to the curve $s=6$. γ_k (left scale) decreases exponentially, loosing roughly a factor 3.5 for $\Delta k=+1$. This is the usually assumed behavior: The lowest orders play the dominant role to determine the parameter γ. However, it is also often inferred from this fact that the lowest orders determine the linewidth. This derivation is wrong as it is demonstrated by the behavior of the parameter $\pi\rho_k^eV_k^e$. As it was shown for SF_6 in Ref. 3, this parameter is first increasing with k, i.e., it has a variation opposite to that of γ_k. The second striking fact is that the curve begins at $k=3$ at a value smaller than 1 ($\pi\rho_3^eV_3^e\sim 0.54$), increases moderately up to a maximum ~ 0.80 at $k=5$, and decreases above, so that the criterion of dissipative redistribution is never checked with $s=s_e=6$. It is noteworthy that $s=6$ corresponds to a four atom molecule, which are known to be excited by IRMPA with great difficulties, the single practical example being BCl_3.[20] In fact, with the previous parameters V_3, a, s, and $2F\bar{v}$, no statistical IVR can occur, although perturbations by intermode couplings become significant. This statistical conclusion must be tempered by the fact that the $2\nu_5$ resonance checks the criterion of strong coupling with the ν_1 mode: $V_e>\Delta\nu$. This is an example of strong but limited redistribution, due to an accidental resonance.

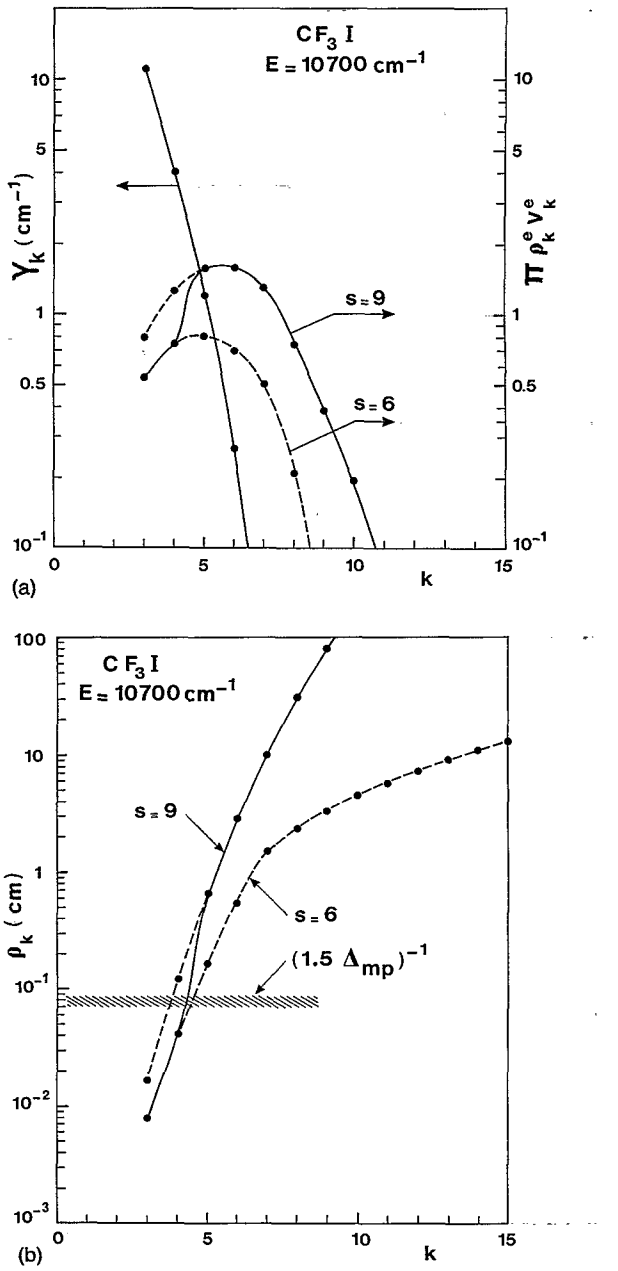

FIG. 6. IVR of a state at $n=10$ ($E=10\,700\ cm^{-1}$) for an equipartition of the energy among the modes. The characteristic quantities of the couplings model are given vs the couplings rank k. (a) Left scale, parameter γ_k; right scale, parameter $\pi\rho_kV_k$ computed with the effective numbers of degrees of freedom $s_e=6$, or the full number $s_f=9$. The jump occurs from $k=4$ to 5 (solid line). (b) Density of coupled states ρ_k computed with $s_e=6$ or $s_f=9$. The jump occurs when the critical density $(1.5\ \Delta_{mp})^{-1}$ is reached (solid line).

As for SF_6, the single way to explain that IVR indeed occurs, is to take into account the full set of degrees of freedom $s=s_f=9$. The passage from s_e to s_f occurs when the quasidegenerate groups of levels are sufficiently split and spread over $\pm\Delta_{mp}$, in such a way that this spreading $2\Delta_{mp}$ checks the following condition [called condition a)]:

$$1.5\Delta_{mp}\rho_k^e \geqslant 1. \tag{20a}$$

In this case, the quasidegenerate groups of levels overlap strongly, so that the full number of degrees of freedom s_f becomes relevant.

Several causes of spreading can be invoked. The first is due to the rotational transitions induced by Coriolis couplings and which extend over $\sim 2B_eJ$. The second is due to the ν_5 splitting $G_{55}(2\bar{l}_5+1)$. The ν_4 splitting can also be present, but as $\nu_4 > \nu_1$, this mode is less involved in resonant transitions. Then we can estimate

$$\Delta_{mp} \sim G_{55}(2\bar{l}_5+1)+2B_eJ. \tag{20b}$$

With $G_{55}=0.65\ \text{cm}^{-1}$ (Ref. 26), $\bar{l}_5=\bar{\nu}_5/2\sim 2.2$, $2B_eJ\sim 5\ \text{cm}^{-1}$ we get $\Delta_{mp}\sim 8.5\ \text{cm}^{-1}$, and then, condition (a) becomes $\rho_k^e > 7.8\ 10^{-2}$ cm. The two curves ρ_k^e ($s=s_e=6$) and ρ_k^f ($s=s_f=9$) are plotted in Fig. 6(b) in semilogarithmic coordinates, with the jump occurring when ρ_k^e overcomes the critical density 7.8×10^{-2} cm. This jump occurs from $k=4$ to $k=5$. We must now be aware that the transformation $\rho_k^e \rightarrow \rho_k^f$ is accompanied by a transformation $V_k^e \rightarrow V_k^f$. It was recalled in Ref. 3 that this transformation obeys the following law. Let

$$R_k = \rho_k^f/\rho_k^e. \tag{21a}$$

Then

$$V_k^f = V_k^e/R_k^{1/2}, \tag{21b}$$

$$\pi\rho_k^f V_k^f = \pi\rho_k^e V_k^e \times R_k^{1/2}. \tag{21c}$$

The identity of Eq. (19) is also immediately derived. The curve $\pi\rho_k^f V_k^f$ is plotted in Fig. 6(a) (curve $s=9$). We observe that at $k=3$, $\pi\rho_3^f V_3^f$ is again smaller than 1, i.e., even with nine degrees of freedom the rank 3 is not able to produce IVR. At $k=5$, when the curve $\pi\rho_k^f V_k^f$ becomes relevant, the value is 1.58 and therefore sufficient to produce a statistical IVR. This value is practically the maximum and for $k\geqslant 8$, the criterion of perturbative redistribution is again checked. Then, we conclude that the dissipative linewidth corresponds to the three orders $k=5$, 6, and 7:

$$\gamma_{\text{diss}} = \sum_{k=5}^{7} \gamma_k \sim 1.5\ \text{cm}^{-1}. \tag{22}$$

We observe that this value is in good agreement with the smaller half-width observed at $E=19\,000\ \text{cm}^{-1}$ (peak e of $^{12}CF_3I$, Table II): $\gamma_e \sim 1.3\ \text{cm}^{-1}$. An intramolecular redistribution time $\tau_{\text{intra}}\sim 1.8$ ps can be derived from Eq. (1c). The maximum number of final states N_k coupled from an initial state is $N_5 \sim N_6 \sim 2.5$ [Eq. (2)]. Then, a given order involves a chain coupling with many steps to ensure the statistical redistribution, one state being coupled to N_k, these ones to N_k^2, and so on. At $E=10\,700\ \text{cm}^{-1}$, the total density of states is $\rho\sim 10^4$ cm (Ref. 20, p. 71). Then, an eigenstate contains about $N_t \sim \pi\rho\gamma_{\text{diss}} \sim 5\times 10^4$ separable states. The number of steps q, necessary to cover all the energy shell, is therefore given by $N_k^q \sim N_t$, i.e., $q\sim 12$, so that about 20 ps are necessary to cover all the manifold. In the previous considerations, only the vibrational transitions have been taken into account. Strong rotational couplings can produce an enhancement of the parameter $\pi\rho_k^e V_k^e$ but with an overall moderate factor; for example, transitions $\epsilon_R=0, \pm 1$ multiply ρ_k^f by 3 and, therefore, $\pi\rho_k^f V_k^f$ by $\sqrt{3}$. All the features analyzed for CF_3I are very close to those obtained for SF_6 in Ref. 3, the major difference lying in the fact that $\pi\rho_k^f V_k^f$ reaches a greater maximum ~ 5 for SF_6, owing to a greater number $s_f=15$. The previous results confirm what was announced by analogy with SF_6: orders $k=3$ and 4 produce only a perturbative redistribution and the order $k=4$ gives lines sufficiently spread out by mode inhomogeneity and multiple transitions to be incorporated in the quasi-Lorentzian formalism through local maxima of γ. The dissipative part corresponds to $k=5,6,7$ and is dominated by the order $k=5$, the resulting γ_{diss} being ~ 1–$1.5\ \text{cm}^{-1}$.

We turn now to the second situation: an overtone state of the ν_1 mode, at the level v_1. This situation is relevant for the discussion of the QC onset, when CF_3I is pumped in the ν_1 mode. It was found in Ref. 3 for SF_6, that the experimental observations were very well fitted using for V_3^e and a_e, the same parameters as those valid for a statistically redistributed state at an energy around the half-dissociation. Then, we use in the modelization, for a heuristic purpose, the same parameters as those of the previous case: $V_3^e=21\ \text{cm}^{-1}$, $a_e=3.75$. The expression of ρ_k is simpler and much more rigorous than for the previous case because the energy $v_1 h\nu_1$ can only be deposited with positive signs in the other modes. It can be stressed that ρ_k is also much smaller, for the same reason, which tends to prevent IVR. It is also important to note that a given order k is related, for quasiresonant exchanges, to a loss of Δv_1 quanta in the pumped mode. The expression ρ_k depends on a scaling factor $1/F'\bar{\nu}(1+\alpha)$ (see Appendix C). F' is of a magnitude ~ 1. We fix F' in the same way as in the previous case, using the experimental data ρ_3^e. It can be remarked that ρ_3^e is in fact, identical to that of the previous case, i.e., $\rho_3^e = 8.14\times 10^{-3}$. ρ_k depends also on the number of bath modes. To be consistent with what follows, we treat the ν_5 mode in connection with the ν_1 mode, because there exists a strong and close resonance $\nu_1/2\nu_5$, which forms a multiplet of entangled levels. We consider therefore the redistribution of this $\nu_1/2\nu_5$ multiplet to the other bath modes, the number of which is $s_b^e=4$. We restrict however to the exchange of ν_1 quanta because the exchange of a group of $2\nu_5$ quanta involves one more quantum and has therefore smaller couplings for a comparable density of coupled states. There can also exist a redistribution of one ν_5 quantum, but the single possibility near resonance is $\nu_5/\nu_3+\nu_6$ with $\Delta\nu=8\ \text{cm}^{-1}$, so that we can have, in fact, a possible multiplet $\nu_1/2\nu_5/\nu_3+\nu_6$. The representation of the bath by $s_b^e=4$ modes is therefore a correct approximation of the reality. The value of γ_k is represented in Fig. 7(a) (left scale, semilogarithmic coordinates). γ_k decreases strongly with a factor ~ 10 for $\Delta k=+1$. The value $\pi\rho_k^e V_k^e$ is plotted also in Fig. 7(a) (right scale, semilogarithmic coordinates) and has a shape quite different from the previous case. It decreases roughly exponentially from a value $\pi\rho_3^e V_3^e \sim 0.54$, smaller than 1, so that the criterion

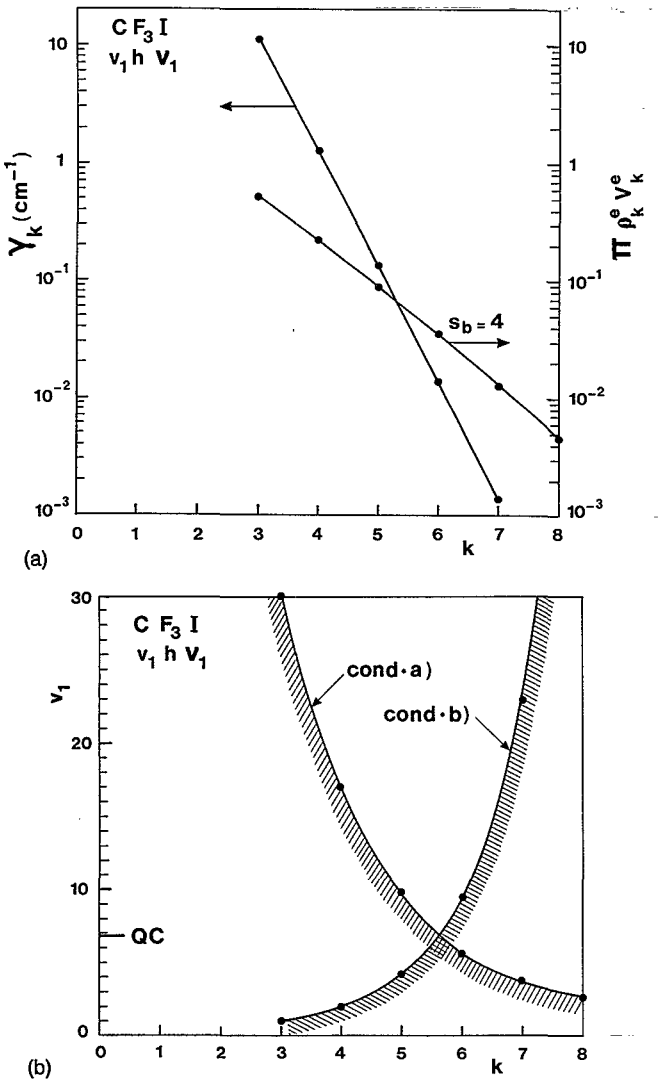

FIG. 7. IVR of an overtone state $v_1 h\nu_1$ vs the couplings rank k. (a) Left scale, parameter γ_k; right scale, parameter $\pi\rho_k^e V_k^e$ computed with the effective number of degrees of freedom in the bath, $s_b^e=4$ (the $2\nu_5$ levels being gathered with the ν_1 levels). (b) Level v_1 for which the full number of individual states is open [condition (a)], and the dissipative IVR criterion $\pi\rho_k^f V_k^f > 1$ is reached [condition (b)]. The minimum minimorum is the QC onset.

of dissipative redistribution is never reached with $s_b^e=4$. We must emphasize that the expression ρ_k is independent on v_1, provided v_1 is sufficiently high to allow the given coupling k, so that the result is valid whatever the overtone v_1 [cf. Eq. (C2)].

To explain the possibility of a dissipative IVR, we must invoke as in the previous case a condition (a) fixing when a greater phase space becomes available, the quasidegeneracy of level groups being removed. The most important cause of spreading lies undoubtedly in the $\nu_1/2\nu_5$ multiplet. One state of such a multiplet at the level $E=v_1 h\nu_1$ can be coupled to a series of state of the multiplet at the level $v_1' = v_1 - \Delta v_1$ with $v_5=2\Delta v_1$, these final states being spread over a range $\pm\Delta_v$. This spreading can be analyzed in the following way. The effective coupling $V^e_{1/5/5}$ between the ν_1 and $2\nu_5$ levels produces, in the harmonic case, a splitting in two components separated by $2V^e_{1/5/5}$. The magnitude of this coupling is given in Fig. 3(a) and the splitting reaches a few tens cm^{-1}. This splitting produces a multiplication of ρ_k^e by the factor $N_{v1}=2$. Now, due to the anharmonic splitting of the ν_5 mode each one of these groups of states is spread over a range $\pm\Delta_{mp}$ which can be estimated by Eq. (20b). Taking into account the degeneracy $g_5=2$, it is easy to see that for a total energy $v_1 h\nu_1$ of the $\nu_1/2\nu_5$ cluster, the average repartition is $\bar{v}_1=v_1/3$ and $\bar{v}_5=4v_1/3$. As for the previous case, we use $\bar{l}_5\sim\bar{v}_5/2$, so that condition (a) for the overlapping of the different clusters is now

$$2[G_{55}(\tfrac{4}{3}v_1'+1)+2B_eJ]N_{v_1}\rho_k^e \gtrsim 1. \tag{23}$$

In this equation, the final state $v_1' = v_1 - \Delta v_1$ is used, Δv_1 depending on k as indicated in Appendix C ($\nu_1\equiv\nu_a$). The condition fixes a minimum v_1 for which the overlapping of the $\nu_1/2\nu_5$ clusters is ensured. This fact produces a multiplication of the density ρ_k^e by the factor R_v^a representing the total degeneracy of the $\nu_1/2\nu_5$ vibrational multiplet, which can be easily computed:

$$R_v^a=(v_1'+1)^2. \tag{24a}$$

We also admit that intramolecular rotational couplings such as the Coriolis interaction produce three possible final states, i.e., ρ_k^e is also multiplied by

$$R_R^a=3. \tag{24b}$$

The density of states becomes $R_v^a R_R^a \rho_k^e$. It will be easily checked that this new density of states is sufficiently high, when Eq. (23) is checked, to be $\gtrsim 1$ cm, so that the spreading of the bath states, dominated by anharmonic terms, exceeds the separation of these clusters. Then, the density of the bath states can be computed with the full number of degrees of freedom $s_b^f=6$ producing an enhancement of the density of states by a factor

$$R_k^b=\rho_k^f(s_b^f)/\rho_k^e(s_b^e). \tag{24c}$$

The condition (b) fixing the onset of dissipative IVR can now be derived [cf. Eq. (21c)] by

$$\pi\rho_k^e V_k^e (R_v^a R_R^a R_k^b)^{1/2} \gtrsim 1. \tag{25}$$

As R_v^a depends on v_1, this equation defines for each k a minimum v_1 allowing the dissipative IVR.

The minima v_1 ensuring conditions (a) and (b) are represented in Fig. 7(b) vs k, using $G_{55}=0.65$ cm^{-1} and $2B_eJ=5$ cm^{-1}. The result is similar to that obtained for SF_6 in Ref. 3. Condition (a) is checked at more and more lower v_1, for k increasing, while the converse is true for condition (b). Then, the onset of the QC is reached when the two conditions are checked. This onset is predicted around $v_1\sim 6.8$ (i.e., $E_{QC}\sim 7300$ cm^{-1}), for k being 5 or 6. This prediction is in good agreement with the experimental Raman monitoring,[6-8] fixing $E_{QC}\sim 6000$ cm^{-1}. Moreover, it is also predicted that the dominant coupling determining the dissipative linewidth is $\gamma_{diss}\sim\gamma_5\sim 0.14$ cm^{-1}. The derived relaxation time is [Eq. (1c)] $\tau_{intra}\sim 20$ ps. It must be emphasized, as for the case of SF_6, that this relaxation time does not correspond to an exponential decrease of the energy from the multiplet $\nu_1/2\nu_5$, but to a loss of $|\Delta v_1|\sim 2$

TABLE V. Parameters determining the redistribution of an overtone CF_3I state $v_1 h\nu_1$ vs the number of quanta exchanged k.

k	Δv_1	ρ_k^e (cm)	γ_k (cm^{-1})	$\pi\rho_k^e V_k^e$	R_k^b	Cond. (a) $v_1 \geqslant$	Cond. (b) $v_1 \geqslant$
3	−1	0.82×10^{-2}	11.3	0.54	2.10	30	1.10
4	−1.33	1.30×10^{-2}	1.28	0.23	2.69	17	1.9
5	−1.66	1.95×10^{-2}	0.137	0.091	3.23	9.9	4.2
6	−2	2.85×10^{-2}	1.42×10^{-2}	0.036	3.60	5.6	9.5
7	−2.33	3.90×10^{-2}	1.38×10^{-3}	0.013	4.23	3.2	23
8	−2.66	5.20×10^{-2}	1.31×10^{-4}	4.6×10^{-3}	4.90	2.7	58
9	−3	6.85×10^{-2}	1.23×10^{-5}	1.62×10^{-3}	5.50	3.0	154

quanta ν_1. This means that a high overtone level, up to $v_1 \sim 15$, can have a relatively slow dissipation of the energy out of the $\nu_1/2\nu_5$ multiplet, at a roughly linear rate of two ν_1 quanta per 20 ps. Although some estimates are fairly crude, we think the main features of the IVR mechanism are understood, explaining either the QC onset or the possibility of relaxation rates on time scales >10 ps. Unfortunately, no picosecond experiments are available for CF_3I, but these time scales were observed for SF_6.[4,5] The different parameters used for the previous computations are gathered in Table V.

From the previous analysis, it appears that the $\nu_1/2\nu_5$ resonance plays a decisive role in the redistribution process, analogous to the degeneracy $g_3=3$ of the ν_3 SF_6 levels, which multiplies the possible relaxation paths. This role has a counterpart in the coherent IRMPA process of the first levels $v_1 \leqslant 6$–7. The presence of a limited redistribution of the $v_1 h\nu_1$ levels on the $2\nu_5$ resonance, and probably also to a less extent on the $\nu_3+\nu_6$ resonance, explains the ease of IRMPA in CF_3I since $3(v_1+1)^2$ pathways become available [Eq. (24)].

In the foregoing, the rotational coupling has been roughly introduced [Eq. (24b)]. Their role is natural since Coriolis couplings are of the order of a few cm^{-1} and compete with ranks of purely vibrational exchanges $k=4$, 5. Without the factor $R_R^a=3$, condition (b) would be obtained at higher v_1, for example 6.0 instead of 4.2 at $k=5$. Increasing number of works shows evidence of the importance of rotational couplings in IVR, especially around the QC onset.[39–42] It should be useful to develop a more accurate model taking into account these rotational couplings and fixing clearly R_R^a, but we think that the main features are reproduced by our analysis. If the number R_R^a increases with k, we can expect that condition (b) be checked at lower v_1 and higher k. This is perhaps the explanation of the recent result of Ref. 43, in which the temporal monitoring of vibrationally excited CF_3I shows signs of IVR on a ~ 1 ns time scale, below the expected QC onset. This IVR can concern only a fraction of states. We see in Table V that $k=6$ and 7 provide values of γ_k giving, respectively, IVR time constants of $\tau_k \sim 200$ ps and 2 ns.

VI. CONCLUSION

Our analysis of the CF_3I QC shows that the same concepts as those used for SF_6 in Ref. 3 explain all existing data. Then the QC of the two benchmark molecules of the IRMPA field seems correctly understood, although our approach cannot pretend to a great accuracy. The analysis of the homogeneous CF_3I spectrum at $E=19\,000$ cm^{-1} leads to a consistent assignment of the main lines, although the presence of the $2\nu_5$ Fermi resonance around 930 cm^{-1} would need a complete and direct observation, not available presently. The hierarchy of couplings V_k appears clearly in this spectrum, demonstrating that the resonances exhibited in low levels spectra keep their identity up to the dissociation threshold.

The width of the peaks in the homogeneous spectrum at $E=19\,000$ cm^{-1} appears dominated by the mode inhomogeneity, i.e., the intramolecular energy repartition among the modes for an isolated molecule, and by multiple transitions of degenerate modes. The resulting half-widths are in the range $\gamma_I \sim 5$–15 cm^{-1}. Out of resonance, the oscillator strength can be treated by a quasi-Lorentzian formalism in which the parameter γ fluctuates locally, the values being dominated by perturbative couplings of rank $k=4$, spread out by mode inhomogeneity and by multiple transitions, and a background of a probably nearly constant contribution γ_{diss} exhibited in the peak e of $^{12}CF_3I$. The spectra at $E=19\,000$ cm^{-1} have finally demonstrated that the anharmonicity can be fitted by a linear variation versus energy up to the half dissociation, but that a strong positive nonlinearity appears above and reaches typically 30% of the linear part. This fact makes the prediction of resonance positions difficult near the dissociation threshold if we know only low levels spectroscopic constants.

The IRMPA process above the QC threshold is now correctly understood, removing the inconsistency of the extraction of the parameter γ from IRMPD data obtained in Ref. 16, which exceeded the observed values by a factor ~ 20. The reasons of this discrepancy are now apparent. Dissociation data are not useful to extract parameters γ, owing to a too much sensitivity to the vibrational distribution tail and to collisional effects or secondary reactions; the ν_4 mode plays a dominant role in the IRMPA process near the dissociation limit because the anharmonicity makes it close to resonance. Finally, an accurate description of the positions and weights of the main resonances ν_1, ν_4, $2\nu_5$, $\nu_2+\nu_3$ leads to a parameter $\bar{\gamma}$, averaged over the vibrational distribution, which has a nice energy dependence, increasing from the QC onset and reaching a plateau around $\bar{\gamma} \sim 5$ cm^{-1}, from $n=10$ up to the dissociation

limit. As for SF_6, the IRMPA process in the QC appears as an out of resonant excitation in the wings of the ν_1 and ν_4 modes, the available oscillator strength being quantitatively dominated by perturbative couplings of rank $k=4$. Nevertheless, the dissipative orders $k\geqslant 5$ are necessary to provide not too small minima of the oscillator strength and to ensure the statistical redistribution of the energy which, in turn, allows the spreading of rank $k=4$ by mode inhomogeneity and multiple transitions.

The hierarchy of couplings has been modelized with a few parameters V_0, a, $F\bar{\nu}$, fixed by the observed ranks $k=3$ and 4. With these parameters, the previous mechanism of IVR, similar to that of SF_6, is stated quantitatively: ranks $k=3$ and 4 are not able to produce a dissipative relaxation, the parameter $\pi\rho_k^e V_k^e$ being smaller than 1 and first increasing vs k, contrary to γ_k. If only degenerate levels are taken into account ($s_e=6$), the dissipative IVR would be impossible whatever the rank k, in agreement with the fact that quadriatomic molecules are nearly unexcitable by IRMPA. Only the spreading of quasidegenerate levels, opening all the phase space [condition (a)] allows the criterion of dissipative IVR for $k=5,6,7$ [condition (b)], and it is apparent that the chain coupling involves a small number of states (~ 3) at each step. This mechanism is responsible for the narrow ultimate linewidth $\gamma_{\text{diss}}\sim 1$–$1.5\ \text{cm}^{-1}$. The IVR from a pumped overtone state exhibits similar features but the density of coupled state at a given order is smaller than in the previous case, leading to a very fast decrease of γ_k vs k. The two conditions (a) and (b) must also be simultaneously checked to ensure dissipative IVR, provided the close resonance with $2\nu_5$ levels be taken into account. This determines a minimum minimorum number of ν_1 quanta fixing the QC onset around $7300\ \text{cm}^{-1}$, in good agreement with the experimental value $\sim 6000\ \text{cm}^{-1}$, owing to the crudeness of the model. The coupling ranks k determining IVR are $k=5,6$ which gives a very narrow dissipative linewidth $\gamma_{\text{diss}}\sim 0.14\ \text{cm}^{-1}$ and an IVR time $\tau_{\text{intra}}\sim 20$ ps. Then, we expect possibilities of selective excitation of the $\nu_1/2\nu_5$ cluster on time scales of a few tens ps, this fact being strengthened by the interpretation of τ_{intra} as a loss of $2\nu_1$ quanta, but not as an exponential relaxation constant.

A striking fact stems from the model, as for SF_6: Data are correctly fitted by a coefficient $a(E)$ of the V_k model very weakly dependent on the energy, from $n=10$ to 18 photons absorbed ($\sim 7\%$ increase). As it was analyzed in Ref. 3, this fact is in contradiction with the usual justification of an exponential decrease of V_k. It is generally argued that the potential $V(x_1,\ldots,x_s)$ can be expressed by a Taylor expansion, the different terms being decreasing with k. Then it can be shown that in this hypothesis,

$$a(E)=V_k/V_{k+1}\propto E^{-1/2} \quad \text{and} \quad \gamma_k(n)\propto n^{k-2},$$

and from $n=10$ to 18 we expect a decrease of 25% for $a(E)$. In the same way, the curve $\bar{\gamma}(E)\sim\gamma_4(E)$, in Fig. 5, is roughly constant from $n=10$ to 18, while we expect from the above formula $\bar{\gamma}(E)\propto E^2$. These remarks show that the Taylor expansion of V is certainly not perturbative, i.e., is not decreasing vs k. The nonseparable part of V corresponds, perhaps, on the contrary to random fluctuations vs $x_1,\ldots,x_s$, and the decrease of the matrix elements vs k must be explained in another way than the usual Taylor expansion. This point will be investigated with more details in further publications.

Although our work is focused on the QC states, the decisive role of the $\nu_1/2\nu_5$ coupling applies also to the lower part, and acts as the ν_3 degeneracy in SF_6 to provide a sufficiently dense set of IRMPA pathways. It is also likely that the previous framework is valid much more generally and can explain, for example, the homogeneous widths $\sim 1\ \text{cm}^{-1}$ observed in C–H or O–H overtone spectroscopies at comparable energies.[44,45]

Very recently, a modelization of a hierarchy V_k,ρ_k has been applied to the IVR in S_1 benzene states[46] and to the so called channel three problem. The author of Ref. 46 used the parameters $V_3=20\ \text{cm}^{-1}$ and $a=10$ and found that the value $\rho_k V_k$ remains smaller than 1 for states $6^1 1^n$ or $7^1 1^n$, implying no statistical mixing. However, if a is replaced by a value comparable to those found for SF_6 and CF_3I in our works, i.e., $a\sim 3$–4, and using the same ρ_k as in Ref. 46, it can easily be checked that $\pi\rho_k V_k$ reaches a maximum value ~ 1.25 at $k=5$, with $\gamma_5\sim 1.5\ \text{cm}^{-1}$ for states $6^1 1^n$, and $\pi\rho_4 V_4\sim 5$, with $\gamma_4\sim 18\ \text{cm}^{-1}$ for states $7^1 1^n$, and the dissipative IVR is explained. This fact suggests a possible universality of the magnitude found for the parameter a in our works.

APPENDIX A: EXPRESSION OF THE SPECTROSCOPIC CONSTANTS

We start from an approximation of the zero order energy:

$$E_0=\sum_i h\nu_i(0)v_i+\sum_i X_{ii}v_i(v_i-1)+\sum_{i<j}X_{ij}v_iv_j + \sum_i G_{ii}l_i(l_i+1)+(A-B)K^2+BJ(J+1). \tag{A1}$$

We derive the part of the transition frequency depending on the total energy

$$v_i(E)=v_i(0)-a_iE+b_iE^2+G_{ii}(2l_i+1)\epsilon_1+2BJ\epsilon_J +2(A-B)K\epsilon_k \tag{A2a}$$

with the selection rules:

$$\epsilon_1=\pm 1, \qquad \epsilon_J=0,\pm 1$$
$$\epsilon_k=0 \qquad \text{for a parallel band}$$
$$\epsilon_k=\pm 1 \qquad \text{for a perpendicular band.} \tag{A2b}$$

For CF_3I, the ν_1 mode is a parallel band ($g_1=1$) and the ν_4 mode a perpendicular band ($g_4=2$). $\nu_i(0)$ is the ground level frequency and a_i can be expressed from the anharmonic constants X_{ij} of the low levels:

$$a_i=\frac{1}{s}\sum_j a_{ij}g_j, \tag{A3a}$$

$$a_{ii}=-\frac{2X_{ii}}{h\nu_i(0)}, \tag{A3b}$$

$$a_{ij}=-\frac{X_{ij}}{h\nu_j(0)} \quad \text{for } i\neq j, \tag{A3c}$$

g_j is the degeneracy of the mode j, s is the total number of vibrational degrees of freedom, and b_i is treated as an adjustable parameter. Equation (7) of the text is derived from Eq. (A2a), as well as an estimate of Δ_{mp}:

$$\Delta_{mp}\sim G_{ii}(2\langle 1_i\rangle+1)+2B\langle J\rangle+2|A-B|\langle K\rangle|\epsilon_k|. \tag{A4}$$

With the spectroscopic constants of Refs. 26–29, $\langle J\rangle\sim\langle K\rangle\sim 50$, $\langle 1_i\rangle\sim 1$–2, and for the ν_1, or ν_4 modes we get $\Delta_{mp}\sim 5$–10 cm^{-1}.

The width of the frequency fluctuations can be expressed by

$$\sigma_{di}=\beta_i(a_iE/2\sqrt{s}) \tag{A5a}$$

with

$$\beta_i^2=\langle|a_{ij}-a_i|^2\rangle_j/a_i^2. \tag{A5b}$$

For CF_3I, $s=9$, and for the ν_1 mode, $a_1=5.2\times10^{-3}$ and $\beta_1\sim\frac{1}{3}$, so that near the dissociation energy, $E_d=19\,000$ cm^{-1}, $\sigma_{d1}\sim 5.3$ cm^{-1}.

Finally, in Eq. (4) of the text, the integrated oscillator strength $\bar{S}_i$ of the resonance i is a constant, for a given mode, and is known from the low level data absorption cross section $\sigma_{a/i}$ (in cm^2):

$$\bar{S}_i=K_i\nu_i(0)=\int d\nu\sigma_{a/i}(\nu). \tag{A6}$$

APPENDIX B: EXPRESSION OF THE IRMPA DISTRIBUTION

The Gaussian approximation $G(n)$, centered in $\langle n\rangle$, is, in the case where the dissociation is neglected,

$$G(n)=\left(\frac{A}{2\pi}\right)^{1/2}\exp\left(-\frac{A}{2}(n-\langle n\rangle)^2\right),$$

with:

$$A=\frac{1}{\langle(\delta n)^2\rangle}=\frac{1}{\bar{a}}\frac{d\bar{a}}{dn}+\frac{1}{\langle n\rangle}\left(\frac{1}{\bar{a}}-1\right),$$

$$\bar{a}=\frac{\rho(\langle n\rangle)}{\rho(\langle n\rangle+1)},$$

where $\rho(n)$ is the density of states computed with a Whitten–Rabinovitch formula.

When the dissociation is no longer negligible, the distribution is a cutoff Gaussian function

$$G_c=\frac{1}{Q}\left(\frac{A}{2\pi}\right)^{1/2}\exp\left(-\frac{A}{2}(n-\bar{n})^2\right) \quad \text{for } n\leqslant n_c,$$

$$G_c=0 \quad \text{for } n>n_c.$$

Q is the normalization factor corresponding to the nondissociated fraction

$$Q=\mathrm{Erf}(x) \quad \text{with } x=A^{1/2}(n_c-\bar{n}).$$

The relation between $\langle n\rangle$ and $\bar{n}$ is

$$\langle n\rangle=n_c+(\bar{n}-n_c)\mathrm{Erf}(x)-(2\pi A)^{-1/2}\exp\left(\frac{-x^2}{2}\right).$$

If $\bar{n}\gg n_c$, $\langle n\rangle=n_c$, and n_c is the maximum possible absorption. For a given $\langle n\rangle$, $\bar{n}$ is computed, with a parameter A as computed previously in $n=\langle n\rangle$. Then G_c is completely defined.

APPENDIX C: EXPRESSIONS OF THE DENSITY ρ_k OF COUPLED STATES AT THE RANK k

1. State with an equipartition of the energy among the modes

The number of modes is s, with an average frequency $\bar{\nu}$. The spreading of the frequencies ν_i around $\bar{\nu}$ is assumed sufficient to give a continuous variation of ρ_k vs the final state energy E'. The doorway state corresponds to a frequency ν_a which we single out. It is assumed that $s<v=E/h\bar{\nu}$. Then

$$\rho_k\sim\frac{1}{F2h\bar{\nu}}N_k\times(S_k)^{1-(k/v)} \tag{C1a}$$

with

$$N_k=\frac{(k-1+s-1)!}{(k-1)!(s-1)!}, \tag{C1b}$$

$$S_k=C_q^p, \tag{C1c}$$

$$p=\frac{\nu_a}{2\bar{\nu}}+\frac{k-1}{2}, \quad q=k-1 \quad \text{if } k<s\leqslant v, \tag{C1d}$$

$$p=\frac{\nu_a}{2\bar{\nu}}+\frac{s}{2}, \quad q=s \quad \text{if } s\leqslant k\leqslant v. \tag{C1e}$$

F takes into account symmetry restrictions and the exact frequency spreading. For p noninteger, functions Γ must be used. For CF_3I and $\nu_a=\nu_1$, we set $\nu_a/\bar{\nu}=\alpha=2$.

2. Overtone states $|v_a,O,\ldots,O\rangle$

We single out the overtone frequency ν_a, while the s_b bath modes have an average frequency $\bar{\nu}$, such that $\nu_a/\bar{\nu}=\alpha$. Then

$$\rho_k=\frac{1}{F'(1+\alpha)h\bar{\nu}}\frac{(\bar{p}+s_b-1)!}{\bar{p}!(s_b-1)!} \tag{C2a}$$

with

$$\bar{p}=\frac{\alpha}{1+\alpha}k. \tag{C2b}$$

$\bar{p}$ corresponds to the number of quanta distributed in the bath modes, around resonance, for $-|\Delta v_a|$ quanta lost by the pumped mode:

$$|\Delta v_a|=\frac{k}{1+\alpha}, \quad |\Delta v_a|+\bar{p}=k, \quad \text{and } v_a\geqslant|\Delta v_a|.$$

[1] C. Angelié, J. Chem. Phys. **96**, 8072 (1992), paper I of this series.
[2] M. Bixon and J. Jortner, J. Chem. Phys. **48**, 715 (1968); J. Jortner and G. C. Morris, J. Chem. Phys. **51**, 3689 (1969).
[3] C. Angelié, J. Chem. Phys. **98**, 2541 (1993), paper II of this series.
[4] R. C. Sharp, E. Yablonovitch, and N. Bloembergen, J. Chem. Phys. **74**, 5357 (1981).
[5] H. S. Kwok, E. Yablonovitch, and N. Bloembergen, Phys. Rev. A **23**, 3094 (1981).
[6] V. N. Bagratashvili, V. S. Doljikov, V. S. Letokhov, A. A. Makarov, L. P. Maljavkin, E. A. Ryabov, E. G. Silkis, and Yu. G. Vainer, Opt. Commun. **38**, 31 (1981).
[7] V. N. Bagratashvili, Yu. G. Vainer, V. S. Dolzhikov, S. F. Kol'yakov, V. S. Letokhov, A. A. Makarov, L. P. Maljavkin, E. A. Ryabov, E. G. Silkis, and V. D. Titov, Sov. Phys.—JETP **53**, 512 (1981).
[8] Yu. R. Kolomiiskii, V. S. Marchuk, and E. A. Ryabov, Sov. J. Quantum Electron. **12**, 1139 (1982).
[9] C. Angelié, R. Capitini, and P. Girard, Laser Chem. **7**, 305 (1987).
[10] O. V. Boyarkin, S. I. Ionov, and V. N. Bagratashvili, Chem. Phys. Lett. **146**, 106 (1988).
[11] S. I. Ionov and A. A. Kobakhidze, Appl. Phys. B **48**, 507 (1989).
[12] O. V. Boyarkin, V. N. Bagratashvili, and C. Angelié, J. Phys. B **25**, 4487 (1992).
[13] C. Angelié, M. Cauchetier, and J. Paris, Chem. Phys. **66**, 129 (1982).
[14] M. Cauchetier, M. Luce, and C. Angelié, Chem. Phys. Lett. **88**, 146 (1982).
[15] C. Angelié, PhD. thesis, University Pierre et Marie Curie, Paris, 1990.
[16] V. N. Bagratashvili, V. S. Dolzhikov, V. S. Letokhov, A. A. Makarov, E. A. Ryabov, and V. V. Tyakht, Sov. Phys.—JETP **50**, 1075 (1979).
[17] M. V. Kuz'min, V. S. Letokhov, and A. A. Stuchebrukhov, Sov. Phys.—JETP **63**, 264 (1986).
[18] A. A. Stuchebrukhov, Sov. Phys.—JETP **64**, 1195 (1986).
[19] A. A. Stuchebrukhov, S. I. Ionov, and V. S. Letokhov, J. Phys. Chem. **93**, 5357 (1989).
[20] V. N. Bagratashvili, V. S. Letokhov A. A. Makarov, and E. A. Ryabov, *Multiple Photon IR Laser Photophysics and Photochemistry* (Harwood, Paris, 1989).
[21] M. F. Goodman, J. Stone, and E. Thiele, in *Multiple Photon Excitation and Dissociation of Polyatomic Molecules*, Chap. 6 of *Topics in Current Physics*, edited by C. D. Cantrell (Springer Verlag, Paris, 1986).
[22] J. Stone, *Lasers, Molecules and Methods* (Wiley, New York, 1989).
[23] J. Stone, E. Thiele, and M. F. Goodman, Chem. Phys. Lett. **71**, 171 (1980).
[24] J. Stone, E. Thiele, and M. F. Goodman, J. Chem. Phys. **75**, 1712 (1981).
[25] K. G. Kay, J. Stone, E. Thiele, and M. F. Goodman, Chem. Phys. Lett. **82**, 539 (1981).
[26] W. Fuss, Spectrochim. Acta **38A**, 829 (1982).
[27] M. O. Bulanin, L. A. Zhigula, T. D. Kolomiitsova, and D. N. Shchepkin, Opt. Spectrosc. **56**, 405 (1984).
[28] H. Bürger, K. Burczyk, H. Hollenstein, and M. Quack, Mol. Phys. **55**, 255 (1985).
[29] D. M. Bishop and L. M. Cheung, J. Phys. Chem. Ref. Data **11**, 119 (1982).
[30] G. L. Peterson and C. D. Cantrell, Phys. Rev. A **31**, 807 (1985).
[31] V. T. Platonenko and N. A. Sukhareva, Sov. Phys.—JETP, **51**, 1065 (1980).
[32] V. N. Bagratashvili, M. V. Kuzmin, V. S. Letokhov, and A. A. Stuchebrukhov, Chem. Phys. **97**, 13 (1985).
[33] A. A. Stuchebrukhov, M. V. Kuzmin, V. N. Bagratasvili, and V. S. Letokhov, Chem. Phys. **107**, 429 (1986).
[34] A. A. Stuchebrukhov and I. E. Khromov, Chem. Phys. Lett. **134**, 251 (1987).
[35] M. Lax, J. Phys. Chem. Solid **25**, 487 (1964).
[36] C. Angelié and Ph. Millié, Chem. Phys. **82**, 171 (1983).
[37] B. Abel, L. Brouwer, B. Herzog, H. Hippler, and J. Troe, Chem. Phys. Lett. **127**, 541 (1986).
[38] B. Abel, H. Hippler, and J. Troe, J. Chem. Phys. **96**, 8863 (1992); **96**, 8872 (1992)
[39] N. Ohta, O. Sekiguchi, and H. Baba, J. Chem. Phys. **88**, 68 (1988).
[40] A. Amirav, Chem. Phys. **124**, 163 (1988).
[41] A. B. Mac Coy, D. C. Burleigh, and E. L. Sibert III, J. Chem. Phys. **95**, 7449 (1991).
[42] P. G. Smith and J. D. Mac Donald, J. Chem. Phys. **96**, 7344 (1992).
[43] M. Quack, R. Schwarz, and G. Seyfang, J. Chem. Phys. **96**, 8727 (1992).
[44] R. H. Page, Y. R. Shen, and Y. T. Lee, J. Chem. Phys. **88**, 4621 (1988).
[45] A. Campargue, F. Stoeckel, and M. Chenevier, Spectrochim. Acta Rev. **13**, 69 (1990).
[46] S. Rashev, J. Chem. Phys. **97**, 2522 (1992).